The Hydromagnetic Interior of a Solar Quiescent Prominence. I. Coupling between Force-balance and Steady Energy-transport.

B. C. Low[1], T. Berger[2], R. Casini[1], & W. Liu[2,3]

ABSTRACT

This series of papers investigates the dynamic interiors of quiescent prominences revealed by recent *Hinode* and *SDO*/AIA high-resolution observations. This first paper is a study of the static equilibrium of the Kippenhahn-Schlüter diffuse plasma slab, suspended vertically in a bowed magnetic field, under the frozen-in condition and subject to a theoretical thermal balance among an optically-thin radiation, heating, and field-aligned thermal conduction. The everywhere-analytical solutions to this nonlinear problem are an extremely restricted subset of the physically admissible states of the system. For most values of the total mass frozen into a given bowed field, force-balance and steady energy-transport cannot both be met without a finite fraction of the total mass having collapsed into a cold sheet of zero thickness, within which the frozen-in condition must break down. An exact, resistive hydromagnetic extension of the Kippenhahn-Schlüter slab is also presented, resolving the mass-sheet singularity into a finite-thickness layer of steadily-falling dense fluid. Our hydromagnetic result suggests that the narrow, vertical prominence H_α threads may be falling across magnetic fields, with optically-thick cores much denser and ionized to much lower degrees than conventionally considered. This implication is discussed in relation to (i) the recent *SDO*/AIA observations of quiescent prominences that are massive and yet draining mass everywhere in their interiors, (ii) the canonical range of 5-60 G determined from spectral-polarimetric observations of prominence magnetic fields over the years and (iii) the need for a more realistic multi-fluid treatment.

Subject headings: MHD — Sun: magnetic fields — Sun: corona — Sun: prominence

---

[1]High Altitude Observatory, National Center for Atmospheric Research, P.O. Box 3000, Boulder, CO 80307, USA

[2]Lockheed-Martin Advanced Technology Center, Solar and Astrophysics Laboratory, 3251 Hanover St., Palo Alto, CA 94304, USA

[3]W. W. Hansen Experimental Physics Laboratory, Stanford University, Stanford, CA 94305

1. Introduction

Quiescent prominences are long-lived, partially-ionized, plasma condensations in the tenuous, million-degree hot, ionized solar corona (Martin, Bilimoria & P. W. Tracadas 1994; Tandberg-Hanssen 1995; Gaizauskas 1998; Labrosse et al. 2010; Mackay et al. 2010). These partially-ionized condensations, at least, their optically-thin observable parts, are typically two orders of magnitude denser and cooler than the surrounding corona. As a macroscopic structure prior to an eruption, a prominence can be remarkably stable, persisting for days to weeks as a long, vertical slab, approximately 5×10^3 km wide, 2×10^4 km tall, 10^5 km long, seemingly suspended by magnetic fields to curve the full prominence length right above and along a magnetic neutral line on the photosphere. By prominence we shall henceforth be referring to this common type, the polar-crown prominence being the canonical example; see the above review articles for a comprehensive view of prominences of all varieties.

Fig. 1 is a *Hinode*/SOT image taken in the Ca II 396.8 nm "H-line" spectral region showing the cool part of the prominence at a high spatial resolution, revealing its characteristic narrow, vertical, dense threads interspersed among narrow, dark lanes. This static image belies the remarkably dynamic nature of these interior structures. Prominence movies from *Hinode* and *SDO*/AIA instruments have established that over internal scales of the order of 300 km and time scales of minutes, these structures are in a constant state of motion at less than free-fall speeds in a characteristic range of $5 - 30$ km s^{-1} (Ahn et al. 2010; Berger et al. 2008, 2010, 2011; Chae et al. 2008; Chae 2010; Liu et al. 2012). The ever-present cool, dense threads are falling whereas the dark lanes among them are narrow streams of hot, tenuous plasma traveling upward at comparable speeds (Berger et al. 2008, 2010). Vertical motions in both directions are actually present in both types of structures, but the high-resolution movies show a discernible average descent of the dense threads and a general bubbly rise of hot, tenuous plasmas. The latter may be the result of rapid heating to coronal temperatures associated with emerging magnetic fluxes that push into the overlying dense prominence material. This condition may be understood in terms of a nonlinear Rayleigh-Taylor hydromagnetic instability (Berger et al. 2010; Hillier et al. 2011). Such emergent-flux structures can be of considerable sizes that first form quasi-statically beneath a quiescent prominence before pushing their ways clear through the prominence without a macroscopic eruption (de Toma et al. 2008; Berger et al. 2011).

A recent quantitative analysis of the motions of descending threads observed with *SDO*/AIA indicates that over a 20 hour period, an order of magnitude more mass may be drained in this manner than found at any one time in a moderate-size, slowly evolving prominence (Liu et al. 2012). Using the lower end of the range of observed prominence densities to compute, the drainage can remove some 10^{15} g from the corona in a day, a mass

comparable to that of a coronal mass ejection. Of particular interest is that the drainage rate estimated from observation is changing in proportion to the slowly-changing, estimated total prominence mass during quasi-steady evolution. This observational result raises two questions. How does the observed significant mass drainage via cool threads relate to the replenishing mass-injection represented by the upward streams of hot, tenuous plasmas? Berger et al. (2011) propose that emerging magnetic flux drives a constant cycling of mass from the photosphere, in the form of tenuous hot plasma, into the coronal cavity overlying a quiescent prominence. This up-flow returns as the draining vertical threads, essentially establishing a 'magneto-thermal' convection as a novel component of the recently recognized chromosphere-corona mass cycle (Marsch et al. 2008; McIntosh et al. 2012).

The other question relates to the embedded magnetic fields in these processes. Spectral polarimetric observations have shown that quiescent prominence plasmas embed typically horizontal, local fields of the order of $5-60$ G (Leroy 1989; Trujillo Bueno et al. 2002; Casini et al. 2003; Lopez Ariste & Casini 2003). These fields are sufficiently intense to dictate the structures of their prominences under a high degree of the frozen-in condition due to high electrical conductivity. In particular, a large amount of mass can be supported by fields of the observed intensities. Yet more mass can drain through the prominence in less than a day than the amount trapped quasi-steadily in the prominence at any one time. How is the observed drainage reconcilable with the observed prominence field being generally horizontal if we accept the frozen-in condition?

An attractive hypothesis is that it is in the nature of prominence dynamics to develop such extreme physical conditions that the usual frozen-in condition breaks down spontaneously. This hypothesis is what we set out to investigate as a theoretical hydromagnetic possibility. The first paper of the series here treats the case of thermal collapse during plasma condensation producing cold, dense, poorly ionized plasmas within which the frozen-in condition cannot be sustained. The second paper takes up a separate piece of physics, demonstrating that despite the high magnetic Reynolds-numbers of the prominence interior, magnetic reconnection takes place readily via spontaneous formation and dissipation of electric current-sheets (Parker 1994; Petrie & Low 2005; Janse, Low & Parker 2010). The two papers provide a hydromagnetic basis to understand the observed restless interior of a prominence.

We digress briefly here to relate our series of papers to other aspects of prominence observations and theory. Observation remains the spearhead in the investigation of quiescent prominences (Berger et al. 2008, 2010, 2011; Chae 2010; Gaizauskas 1998; Heinzel et al. 2008; Labrosse et al. 2010; Lites et al. 2010; Mackay et al. 2010; Martin, Bilimoria & P. W. Tracadas 1994; Martin & Panasenco 2010; Tandberg-Hanssen 1995; Okamoto et al. 2007,

2008; Okamoto, Tsuneta & Berger 2010; Reeves et al. 2012; van Ballegooijen 2004). Presently not all the observed properties in prominences can be theoretically understood or understood in a unified way. For example, the sub-arcsecond threads, revealed by ground-based, high-resolution, static H_α images of on-disk prominences, have remained difficult for theory to unify with the space observations of prominences at the solar limb described above (Zirker, Engvold & Martin 1998; Lin, Engvold & Wiik 2003; Lin et al. 2005; Su et al. 2011). These two views of prominence structures have also not been reconciled with the polarimetric observations of prominence and coronal magnetic fields (Leroy 1989; Casini et al. 2003; Casini & Judge 1999; Judge, Low & Casini 2006; Lopez Ariste & Casini 2003; Tomczyk et al. 2008; Trujillo Bueno et al. 2002; Dove et al. 2011).

Observations can pose good physical questions to be addressed theoretically in their own rights, without necessarily aiming at a comprehensive explanation of all the rich observations. In the face of many unanswered questions, our series of paper seeks to build up our intuition for seeing the complex observations in terms of the elementary physical principles. Previous works of this kind have addressed magnetic support of the prominence weight under the frozen-in condition using 2D and 3D field models with energy transport greatly simplified or ignored for the sake of tractability (Aulanier, DeVore & Antiochos 2002; Chae 2010; Low & Hundhausen 1995; Low & Zhang 2004; Low & Petrie 2005; Lopez Ariste et al. 2006; Manchester et al. 2004; Petrie & Low 2005; Priest, Hood & Anzer 1989; Régnier & Amari 2004; van Ballegooijen 2004; Wu & Low 1987). In complement, models of 1D sophisticated energy transport along field lines, prescribed to be fixed in space, made progress with insights into the condensation processes by suppressing the dynamical interaction of the field with energy transport (Karpen, Antiochos& Klimchuk 2006; Karpen & Antiochos 2008; Xia et al. 2011; Luna, Karpen & Devore 2012). This dynamical interaction is the subject of a recent time-dependent MHD simulation by Xia, Chen & Keppens (2012) demonstrating the self-consistent formation of a magnetic dip where a prominence results from heating and condensation. Heasley and Mihalas (1976) pioneered studying the coupling of radiative transfer to the equilibrium forces in a slab model; see also Anzer & Heinzel (1999). Allowing for gravity and a heuristic approximation of the Lorentz force, Heasley and Mihalas encountered an inevitable presence of collapsed mass-sheets. Their mass-sheet is, perhaps, a rudimentary form of the singularity in the KS-slab model investigated in our first paper here.

Specifically we treat the following theoretical problem. We construct a complete family of exact solutions describing a vertical Kippenhahn-Schlüter (KS) plasma-slab supported against gravity in a bowed magnetic field in unbounded space, varying only in the direction perpendicular to the slab (Kippenhahn & Schüter 1957; Low 1975; Hillier et al. 2011). We assume static force equilibrium under (i) the frozen-in condition and (ii) a steady balance

among optically-thin radiation, heating, and thermal conduction directed along the field. These three energy processes take the theoretical forms studied by Low & Wu (1981), representing an energy transport of a minimum physical complexity relevant to prominences. Despite its one-dimensionality, the KS slab captures important properties of this complex system. The novel result of the study is that the set of everywhere-analytical solutions found in the earlier study is only a subset of measure zero of all the physically admissible equilibrium states of the KS slab. Generally, force-balance and steady energy-transport cannot both be met under the frozen-in condition without a fraction of the total mass of the slab having collapsed into a mathematical singularity representing an exceedingly cold, dense sheet at the center of the otherwise diffuse slab. The weight of that mass sheet is supported by a discrete Lorentz force due to a discrete electric current in the sheet. This discrete current can be maintained only if the frozen-in condition is rigorously obeyed, that is, the electrical conductivity is infinite. The electrical conductivity in the solar atmosphere is large but finite, of course. In that case, an evolution to equilibrium must at first seek a state with an inevitable singularity when the frozen-in condition does apply to a very high degree. As the singularity develops, the small nonzero electrical resistivity unavoidably becomes significant at a point in time, resulting in current dissipation. A breakdown of the frozen-in condition thus occurs spontaneously.

The general inevitability of mass-sheet singularity in the KS-slab is demonstrated in Section 2. The singular equilibrium solutions containing a mass sheet with a discrete current are analyzed in Section 3. The breakdown of the frozen-in condition is illustrated in Section 4, treating an exact solution for a steady, vertical resistive hydromagnetic flow and pointing out the need for a more realistic multi-fluid description. Our results are summarized in Section 5 to relate in general terms to the physics of prominences. The cgs units are used throughout the paper.

2. Coupling between static force-balance and steady energy-transport

We adopt a one-fluid hydromagnetic description of the corona and prominence:

$$\rho\left[\frac{\partial \mathbf{v}}{\partial t}+(\mathbf{v}\cdot\nabla)\,\mathbf{v}\right] = \frac{1}{4\pi}(\nabla\times\mathbf{B})\times\mathbf{B}-\nabla p-\rho g\hat{z}, \tag{1}$$

$$\frac{\partial \mathbf{B}}{\partial t} = \nabla\times(\mathbf{v}\times\mathbf{B}-\eta\nabla\times\mathbf{B}), \tag{2}$$

coupling the velocity $\mathbf{v}$ to the magnetic field $\mathbf{B}$; ρ, p, and g being the density, pressure and uniform gravitational acceleration in the negative Cartesian-z direction. The coefficient of resistivity $\eta = c^2/4\pi\sigma$ is generally very small over all observable length scales in the sense

of a large magnetic Reynolds-number $R_M = v_0 l_0/\eta$, c and σ being the speed of light and electrical conductivity, respectively, and, v_0 and l_0 denoting characteristic speed and length, respectively. The time $\tau_D = l_0^2/\eta$ for a magnetic structure of characteristic length l_0 to diffuse resistively is another indicator of the importance of resistive effects. Set $l_0 \approx 7 \times 10^7$cm as the limit of spatial resolutions achievable with a ground-based telescope. Then the Spitzer (1962) resistivity $\eta = 3 \times 10^{12}\ T^{-3/2}$ cm^2 s^{-1}, where T is the temperature, gives τ_D well in excess of tens of years or longer for temperatures in the range of $10^4 - 10^6$K. Therefore, the frozen-in condition can only break down if a hydromagnetic fluid develops exceedingly small scale structures. In the case of the corona, these scales may even fall below the mean free path of the fluid, so that the applicable resistivity involves coupling between the large-scale fluid and particle-kinetic effects (Low et al. 2012).

We are interested in a static equilibrium with a negligible η, so that currents may persist permanently. Then, setting $\mathbf{v} = 0$, the induction equation (2) is irrelevant except to demand that $\mathbf{B}$ is solenoidal. The mass-conservation equation is also irrelevant, and static equilibrium is described by the complete set of equations:

$$\frac{1}{4\pi}(\nabla \times \mathbf{B}) \times \mathbf{B} - \nabla p - \rho g \hat{z} = 0, \tag{3}$$

$$\nabla \cdot \mathbf{B} = 0, \tag{4}$$

$$\nabla \cdot \left[\kappa \frac{(\mathbf{B} \cdot \nabla T)\,\mathbf{B}}{|\mathbf{B}|^2}\right] - r(\rho, T) + h(\rho, T) = 0, \tag{5}$$

$$p = \frac{k_B}{m_0}\rho T, \tag{6}$$

where we introduce the ideal gas law, with k_B and m_0 being the Boltzmann constant and the mean mass of the fluid particles, respectively. Force-balance equation (3) is coupled to steady energy equation (5). The latter balances radiative loss r, heat gain h and a thermal conductive flux aligned along $\mathbf{B}$ with a thermal conductivity κ. The properties of a specific plasma fluid is represented by r, h and κ as known functions of the thermodynamic variables, p, ρ and temperature T.

This radiative magnetostatic problem is formidable, especially for a three-dimensional system. We therefore treat a localized one-dimensional system. To keep physical issues in mind we first briefly describe the model in relation to the real prominence and its surrounding. Then we formulate the mathematical problem in Section 2.1 and show in Section 2.2 that the physically complete set of solutions must include both everywhere-analytic solutions as well as the solutions with admissible singularities presented in Section 3.

The prominence in Fig. 1 belongs to a larger-scale, three-part coronal helmet-streamer of the kind in the white-light image of a total eclipse in Fig. 2. Coronal observation of

the magnetic fields external to prominences in the corona is still in its infancy (Casini & Judge 1999; Judge, Low & Casini 2006; Tomczyk et al. 2008; Dove et al. 2011), but it is physically reasonable to interpret a helmet-streamer to be an arcade of closed magnetic field anchored with magnetic footpoints frozen into the base of the corona (Low 1996, 2001; Zhang & Low 2005). This field traps the high density of the helmet-streamer in approximate static equilibrium under the frozen-in condition. External to the helmet-streamer is the solar wind accelerated from quasi-static conditions at the coronal base. This wind combs its frozen-in fields into an open configuration, each field line extending from one footpoint anchored in the coronal base out into the heliosphere. The bright helmet often has a tenuous, dark cavity at its base within which a quiescent prominence can be found located at the bottom of that cavity. When the line of sight is aligned favorably with the arcade of the helmet-streamer, an exemplary case in Fig. 2, this three-part structure is seen clearly.

Observations support the interpretation that the cavity is a magnetic flux rope with field lines that wind around within that cavity (Fan 2001; Manchester et al. 2004; Zhang & Low 2005; Cottaar & Fan 2009). The prominence may then be explained as the cool condensed plasma trapped at the bottom of local U-shaped flux tubes under a high degree of the frozen-in condition (Fan & Gibson 2006, 2007; Fuller et al. 2008; Gibson & Fan 2006; Gibson 2010; Schmit et al. 2009; Schmit & Gibson 2011). The frozen-in condition permits no motion of the condensation across magnetic flux surfaces. Our study here sets out to first understand this frozen-in state well, only to discover from the physics of such a state that the frozen-in condition must generally break down in the prominence interior to produce cross-field transport of mass at less than free-fall speeds.

2.1. A thermally-balanced Kippenhahn-Schlüter slab

Consider a 1D system that depends on only the Cartesian coordinate y. Let the field have the solenoidal form:

$$\mathbf{B} = B_0 \left[G_0, 1, H(y)\right], \tag{7}$$

B_0 and G_0 being constants. We are interested in $B_z = B_0 H(y)$ being a monotonically-increasing, odd function with $H = 0$ at $y = 0$. This field is deformed from a uniform "background" field

$$\mathbf{B}_{bg} = B_0 \left[G_0, 1, 0\right], \tag{8}$$

by weighing upon it with frozen-in mass, producing a bow-shape geometry to represent a local U-shaped field. In this idealized unbounded domain, the surrounding prominence environment tends to a uniform state located at $y \to \pm\infty$.

Introduce the dimensionless variables,

$$P = p/p_0, \quad D = \rho/\rho_0, \quad \theta = T/T_0, \quad Y = \frac{y}{\Lambda_0}, \tag{9}$$

where $\Lambda_0 = \frac{k_B T_0}{m_0 g}$ is the hydrostatic density scale height at temperature T_0 related to the other normalization constants by $p_0 = \rho_0 k T_0/m_0$. The ideal gas law is then

$$P = D\theta. \tag{10}$$

Introduce the two plasma β-parameters:

$$\beta = \frac{8\pi p_0}{B_0^2}, \tag{11}$$

$$\beta_{net} = \frac{8\pi p_0}{B_0^2\left(1 + H(Y)^2 + G_0^2\right)} < \beta, \tag{12}$$

respectively measuring the importance of the fluid pressure relative to the magnetic pressures of the uniform $B_y = B_0$ and the total field $|\mathbf{B}| = B_0\left(1 + H^2 + G_0^2\right)^{1/2}$. With no loss of generality, take $p = p_0$ to be the pressure at the center of the sheet, ie, $P = 1$, $H = 0$ at $Y = 0$. Then, the force-balance equation (3) reduces to the y and z components:

$$\beta P + H^2 = \beta, \tag{13}$$

$$\frac{dH}{dY} = \frac{1}{2}\beta D. \tag{14}$$

Equation (13) shows that the total pressure $p + B^2/8\pi$ is uniform in space which is a sufficient condition for linear hydromagnetic stability (Zweibel 1982). The high pressure of the sheet is confined by the vertical component $B_z = B_0 H$ significant outside the sheet. Equation (3) can be written in the form

$$\frac{1}{4\pi}\left(\mathbf{B}\cdot\nabla\right)\mathbf{B} - \nabla\left(p + \frac{B^2}{8\pi}\right) - \rho g\hat{z} = 0, \tag{15}$$

in terms of the magnetic tension and the total-pressure force. Since the total pressure of the KS-slab is uniform in space, the tension force is everywhere vertical and it alone supports the weight of the plasma. In other words, the left hand side of Equation (14) is essentially the upward magnetic tension force.

We pause to relate the above idealized magnetic field to spectral-polarimetric observations of prominences. If we identify the concentration of plasma around $Y = 0$ with the prominence plasma being observed, where $B_z = B_0 H \approx 0$, polarimetric observation will detect the horizontal field $\mathbf{B}_{bg}$ given by Equation (8). The observed field has intensity $B_0\left(1 + G_0^2\right)^{1/2}$ which can fall within the observed range of $5 - 60$ G even with B_0 small as

long as G_0 is sufficiently large. Therefore, the plasma-beta β given by Equation (11) may be larger than unity whereas the plasma-beta β_{net} defined by Equation (12) in terms of the net field is typically less than unity. This feature simply reflects the fact that a slab of plasma hemmed up by a background field aligned close to the central plane of the slab will snag only a weak component B_y of the field across it. Therefore, the field would sag greatly in the $y-z$ plane with a large value of β.

We take advantage of this simplicity of the model to deal with the complexity of thermal balance. We adopt the temperature-dependent Spitzer (1962) thermal conductivity

$$\kappa = \kappa_S \; T^{5/2} \; erg \; cm^{-1} s^{-1} K^{-1}, \tag{16}$$

for a fully ionized gas where $\kappa_S = 2 \times 10^6$. For our theoretical purpose, we adopt this conduction model in a formal sense with κ_S taken as an ad hoc constant, so as to be conceptually specific about the model of thermal conduction adopted. To complete the specification of the fluid's material properties, we take

$$r = \alpha_0 \rho^2 T, \tag{17}$$

$$h = \gamma_0 \rho, \tag{18}$$

where α_0 and γ_0 are constants characteristic of the fluid. Here we model radiative loss r to be optically thin, collisional in nature as represented by its quadratic dependence on density. Detailed radiative calculations have shown that the collisional r has this form with α_0 approximately constant in contiguous ranges of temperatures from 10^4K to 10^6K, multiplied by a monomial in T of a constant power in each of those ranges (Tandberg-Hanssen 1995). In Equation (17) we take α_0 to be constant and the temperature factor to be linear in T to simplify an otherwise very complex mathematical problem. The origin of heating in the prominence is poorly understood, representing another uncertainty in such thermal models. For our theoretical study we use an ad hoc heating rate proportional to density (Uchida 1963; Tandberg-Hanssen 1995). These choices lead to an analytically integrable model (Low & Wu 1981). We wish to investigate this model afresh to understand the physical meaning of these analytical solutions.

With the material properties of the plasma fluid so specified, energy equation (5) takes the dimensionless form:

$$\frac{d}{dY}\left[\frac{\kappa_0 \theta^{5/2}}{1+G_0^2+H^2}\frac{d\theta}{dY}\right] = D^2\theta - \gamma D, \tag{19}$$

where

$$\gamma = \frac{\gamma_0 k_B}{\alpha_0 m_0 p_0} = \frac{8\pi\gamma_0 k_B}{\alpha_0 m_0 B_0^2}\frac{1}{\beta}, \tag{20}$$

$$\kappa_0 \;=\; \frac{\kappa_S T_0^{5/2}}{\alpha_0 \rho_0^2 \Lambda_0^2}, \tag{21}$$

Λ_0 being the scale height at temperature T_0 already introduced. Equation (19) as a second order ODE requires two boundary conditions to determine θ. We choose them to be

$$Y \;= 0, \quad \frac{d\theta^{7/2}}{dY} = 0, \tag{22}$$

$$Y \;\to \infty, \quad \frac{d\theta^{7/2}}{dY} \to 0. \tag{23}$$

Condition (22) comes from the assumed symmetry of $\theta(Y)$ about $Y = 0$. Since the heating source is explicitly accounted for by h, condition (23) sets the thermal flux to vanish at infinity. In the unbounded model considered here, the h-heating and r-radiation vanish at infinity. An external source of thermal flux coming in from infinity would require an unphysical temperature that increases to unbounded values at infinity. An external sink of thermal flux at infinity is incompatible with the unbounded domain, since a monotonically decreasing temperature must become zero at some finite Y on either sides of $Y = 0$. The h-heating is the only source of energy in this magnetostatic atmosphere with thermal conduction transporting excess heat to where it can be radiated away. The equations (10), (13), (14), and (19) are a complete set of scalar equations for the dependent variable P, D, θ, and H. In principle, Equations (10), (13), and (14) determine P, D and H in terms of θ so that Equation (19) determines θ as a function of Y subject to the two homogeneous boundary conditions (22) and (23). From the solution $\theta(Y)$ obtained, the other dependent variables can then be expressed as functions of Y.

The model is 1D only in the mathematical sense. The field is sheared and bowed in 3D space. This 3D geometry strongly influences energy-balance, represented by the factor $(1+G_0^2+H^2)^{-1}$ in Equation (19). The thermal flux is completely aligned along the field. This factor depends on the magnitudes of the two field components, $B_x = B_0 G_0$ and $B_z = B_0 H$. For large values of G_0 and H, respectively describing high magnetic shear and great sag in the field, the thermal flux enters the plasma slab at a large oblique angle.

2.2. The physically complete set of solutions

The governing Equations (10), (13) and (14) and (19) can be reduced to a quadrature. This was shown by Low & Wu (1981) using P as an independent variable and D, θ, H and Y the dependent variables. In that formulation, D, θ, H can be solved analytically explicitly in terms of P, following which solving Y as a function of P gives the distributions of the

equilibrium field and plasma in space. Here we take a different approach, choosing H instead of P as the independent variable.

By Equation (14) describing the vertical balance of force in a slab symmetrical about $Y = 0$, $H(Y)$ must be monotonically increasing in the domain $-\infty < Y < \infty$ since density $\rho = \rho_0 D$ is positive. Define $H(\pm\infty) = \pm H_0$, and Equation (13) gives $H_0 = \sqrt{\beta}$ with $P(\pm\infty) = 0$. The total mass M in an infinitely long column, of unit cross-sectional area, parallel to the Y-axis is given by

$$\begin{aligned} Mg &= \rho_0 \Lambda_0 g \int_{-\infty}^{\infty} D dY \\ &= \frac{2p_0}{\beta} \int_{-\sqrt{\beta}}^{\sqrt{\beta}} dH \\ &= \frac{B_0^2}{2\pi} \sqrt{\beta}. \end{aligned} \tag{24}$$

Hereafter we called M simply the total mass. During an evolution of this 1D system, M is a constant in time. When this system is in equilibrium in a background field with a given B_0, M determines $\beta = 8\pi p_0/B_0^2$ by Equation (24). In other words, M determines the central fluid pressure $p(0) = p_0$ and the far vertical field component $B_z(\pm\infty) = \pm B_0 H_0$, recalling $H_0 = \sqrt{\beta}$. The greater the total mass the greater is the sag of the field with a large far vertical component and a high pressure p_0 at the bottom of the V-shaped field.

We now pose the following mathematical problem. Equation (13) gives $P(H)$ explicitly. If $\theta(H)$ is also known, $D(H)$ is given by the ideal gas law (10). Then solving Equation (14) for $H(Y)$ not only determines $\mathbf{B}(Y)$ but also gives $P(Y)$, $\theta(Y)$, and $D(Y)$. Therefore, the problem posed starts with determining $\theta(H)$ in the domain $|H| \leq H_0 = \sqrt{\beta}$ for a specified β. In other words, we need to transform energy equation (19) as a differential equation for θ from domain $|Y| < \infty$ to an equation in the domain $|H| \leq H_0 = \sqrt{\beta}$. Let us carry out such a transformation and solve for $\theta(H)$ in the three-step development below, leading to a family of physically complete solutions, the meaning of "physically complete" becoming clear at the end of the construction.

2.2.1. The isothermal KS slab and related simple models

It is instructive to consider the isothermal solutions, treated by Kippenhahn and Schlüter (1957). Such a state arises if the fluid does not radiate, $\alpha_0 = 0$, and is not heated, $\gamma_0 = 0$, but is thermally conducting $\kappa_S \neq 0$. Then with $\theta = \theta_1$, a constant, and $P = \theta_1 D$, Equation

(14) can be integrated to give the isothermal solution:

$$H = \sqrt{\beta}\tanh\frac{\sqrt{\beta}}{2\theta_1}Y, \tag{25}$$

$$D = \frac{1}{\theta_1}\mathrm{sech}^2\frac{\sqrt{\beta}}{2\theta_1}Y. \tag{26}$$

The field lines in 3D space has uniform $B_x = B_0 G_0$ and each projects into the bowed curve in the $Y - Z$ plane:

$$Z - Z_0 = 2\theta_1 \log\cosh\frac{\sqrt{\beta}}{2\theta_1}Y, \tag{27}$$

identified by its crossing the axis $Y = 0$ at $Z = Z_0$ in normalized unit Λ_0. This isothermal solution is displayed in Fig. 3.

Along the projected field line, the invariant frozen-in mass M is distributed hydrostatically, decreasing with Z exponentially with a scale height $\Lambda_0\theta_1$; recall that θ_1 is temperature in units of the free normalization constant T_0. This exponential decrease with height combined with the self-consistent shape of the field line renders the pressure P a strict function of Y, seen in the following two equivalent expressions,

$$\begin{aligned} P &= \mathrm{sech}^2\frac{\sqrt{\beta}}{2\theta_1}Y \\ &= \exp\left(\frac{Z_0 - Z}{\theta_1}\right), \end{aligned} \tag{28}$$

the latter giving P varying with height Z along a fixed field line identified by the constant value Z_0. As a function of Y, P has a width proportional to the scale height $\Lambda_0\theta_1$ and inversely proportional to the total mass M, with $\sqrt{\beta}$ related to M by Equation (24). With the background field $\mathbf{B}_{bg}$ fixed, the greater M is, the greater would be the sag in the field, and, hence, the narrower would be the peaks of P and its isothermal density D.

On a scale large compared to the pressure width, we only see the two uniform-field parts of the bowed field lines on two sides of $Y = 0$. The mass concentration centered at $Y = 0$ appears as a sheet of zero thickness on such a scale. On the other hand, letting θ_1 go to zero decreases the scale height $\Lambda_0\theta_1$ and the width of the mass concentration both to zero in absolute measure of length. This happens, for example, in a fluid that is not heated but constantly radiating away energy, with a very high thermal conductivity to keep the temporally decreasing θ_1 uniform in space. If we fix β in this process, the total mass M is unchanged. In the limit $\theta_1 \to 0$, D becomes proportional to $\delta(Y)$, the Dirac delta function accounting for the unchanging mass M. At the same time, H given by Equation (25) tends to a step function jumping from $-\sqrt{\beta}$ to $\sqrt{\beta}$ upon crossing $Y = 0$ from the left. The pressure

changes such that $P = D\theta_1 \to 1$ at $Y = 0$ for all time but vanishingly small for all points $Y \neq 0$, self-consistently describing a cold thin sheet of mass in pressure equilibrium with the external magnetic field. In these considerations physics dictates that fluid and magnetic pressures must always be bounded whereas density may grow unboundedly so long as its integral gives a bounded mass. This narrowing of the density peak with a fixed total mass combined with a vanishingly small temperature illustrates a form of thermal collapse relevant to Section 2.2.3.

Two related properties are worthy of mention when the temperature varies in space. Equilibrium requires $B_z = B_0 H(Y)$ to be monotonically increasing in $-\infty < Y < \infty$. This ensures the pressure is positive and monotonically decreasing with Y. It also ensures the density is positive but does not require the density to be a monotonically decreasing function of Y. Depending on the variation of the temperature with Y, the density may have two maxima located off the center $Y = 0$, rather like the density inversion layer in a vertical atmosphere (Lerche & Low 1980a). The other property is that in the unbounded space, energy balance may be such that the pressure P declines with Y to become zero at some finite distance $Y = \pm Y_0$ external to which $P = D = 0$. The mass sheet has condensed and contracted to a finite width rather like a vertical atmosphere with a finite top above which is vacuum (Lerche & Low 1980a).

2.2.2. The everywhere-analytical solutions of Low & Wu

Let us transform energy equation (19) in Y-space into its equivalent,

$$\frac{1}{10}\kappa_0\beta^2\frac{d}{dH}\left[\frac{\beta - H^2}{1 + G_0^2 + H^2}\frac{d\theta^{5/2}}{dH}\right] = \beta(1-\gamma) - H^2, \tag{29}$$

in H-space, using Equations (10), (13) and (14) to remove explicit dependance on Y. The term within the square brackets on the left side of Equation (29) is essentially the thermal flux along the field. Introduce the dimensionless thermal flux $\mathcal{F}$ defined by

$$\mathcal{F} = \frac{1}{2}\beta^2\kappa_0\frac{\theta^{5/2}}{1 + G_0^2 + H^2}\frac{d\theta}{dY}. \tag{30}$$

Removing the explicit Y-dependence from its right hand side, we rewrite this definition as

$$\mathcal{F} = \frac{1}{10}\beta^2\kappa_0\frac{\beta - H^2}{1 + G_0^2 + H^2}\frac{d\theta^{5/2}}{dH}, \tag{31}$$

so that Equation (29) takes the form

$$\frac{d\mathcal{F}}{dH} = \beta(1-\gamma) - H^2, \tag{32}$$

with the integral

$$\mathcal{F} = \frac{1}{3}H\left[3\beta(1-\gamma) - H^2\right] + H_1, \tag{33}$$

H_1 being an integration constant. A second integration using Equation (31) then gives

$$\begin{aligned}\frac{3}{5}\beta^2\kappa_0\left(\theta^{5/2} - \theta_2^{5/2}\right) = \\ 6H_1\left(\sqrt{\beta} - H\right) + \left[(2-3\gamma)\beta - \Gamma_0\right](\beta - H^2) + \frac{1}{2}(\beta - H^2)^2 \\ - \Gamma_0\left[3\frac{H_1}{\sqrt{\beta}} + (2-3\gamma)\beta\right]\log\left(\sqrt{\beta} - H\right) \\ + \Gamma_0\left[3\frac{H_1}{\sqrt{\beta}} - (2-3\gamma)\beta\right]\log\left(\sqrt{\beta} + H\right),\end{aligned} \tag{34}$$

where $\Gamma_0 = 1 + G_0^2 + \beta$ and θ_2 is an integration constant.

The homogenous boundary conditions (22) and (23) require $\mathcal{F} = 0$ at $H = 0$ and $H = H_0 = \sqrt{\beta}$ in the H-domain, leading to $H_1 = 0$ and $\gamma = 2/3$ and the solution

$$\theta^{5/2} = \theta_2^{5/2} - \frac{5}{3\beta^2\kappa_0}\left(1 + G_0^2 + \frac{1}{2}\beta + \frac{1}{2}H^2\right)(\beta - H^2), \tag{35}$$

the everywhere analytical solution of Low & Wu (1981). The free integration constant θ_2 is the temperature at $H = \pm\sqrt{\beta}$ corresponding to $Y \to \pm\infty$. The temperature decreases inward monotonically to the temperature θ_1 at $Y = H = 0$ given by

$$\theta_1^{5/2} = \theta_2^{5/2} - \frac{5}{3\beta\kappa_0}\left(1 + G_0^2 + \frac{1}{2}\beta\right). \tag{36}$$

The integration constant θ_2 is arbitrary but is physically required to be positive and bounded below such that $\theta_1 \geq 0$. Let us replace θ_2 with θ_1 as the arbitrary integration constant, with no loss of generality.

Our boundary value problem with its homogeneous boundary conditions is a nonlinear eigenvalue problem that admits only one value, 2/3, for the eigenvalue γ. We use the notation $\gamma_c = 2/3$ whenever we mean 2/3 as a special number in this sense. The eigenfunction $\theta^{5/2}$ corresponding to $\gamma = \gamma_c$ is highly degenerate, that is, there is an infinity of eigenfunctions, corresponding to the second free integration constant $\theta_1^{5/2}$ not fixed by the boundary conditions. For each member of this infinite set of solutions in the H-domain, defining the temperature θ, the governing Equations (10), (13) and (14) can be used to construct the corresponding spatial distributions of field and fluid.

The eigenvalue $\gamma = \gamma_c$ is set by the global balance of energy. Homogenous boundary conditions (22) and (23) describe a closed thermally-conducting system. As we have pointed

out, thermal conduction is not a source of energy in this unbounded domain, serving only to conduct heat to balance the total heat input $\mathcal{H}$ against the total radiational loss $\mathcal{R}$. These two quantities can be explicitly evaluated in the H-domain:

$$\begin{aligned} \mathcal{H} &= \gamma \int_{-\infty}^{\infty} D dY \\ &= \frac{4\gamma}{\sqrt{\beta}}, \end{aligned} \tag{37}$$

$$\begin{aligned} \mathcal{R} &= \int_{-\infty}^{\infty} D^2 \theta dY \\ &= \frac{8}{3\sqrt{\beta}}, \end{aligned} \tag{38}$$

with the ratio

$$\frac{\mathcal{H}}{\mathcal{R}} = \frac{2}{3}\gamma. \tag{39}$$

The eigenvalue $\gamma = \gamma_c = 2/3$ follows from $\mathcal{H} = \mathcal{R}$ for global energy balance, described by a whole family of everywhere-analytical solutions distinguished by the temperature θ_1 at $Y = 0$.

Fig. 4 shows two representative solutions for $\beta = 5.0$ but differing in $G_0 = 0.0$ in case (a) and $G_0 = 200$ in case (b), each case with a thermal conductivity κ_0 prescribed so that the temperature rises from some central temperature $\theta = \theta_1$ at $Y = 0$ to a hundred times higher temperature $\theta = \theta_2$ at $Y \to \infty$. The constant β fixes the amount of frozen-in mass M, the same for both cases, whereas G_0 determines the obliqueness of the field-aligned, thermal-conductive flux supplying energy to the central part of the slab. The thermal conductivity effectively is geometrically reduced in case (b) with its highly sheared field, compared to case (a) with the field lying in the $Y - Z$ plane. The reduction of thermal conduction influences both the stratification and thermal structure, since energy-transport and force-balance are nonlinearly coupled. Thus, the steepening of the thermal gradients around the central temperature minimum in case (b), relative to case (a), is accompanied by the total mass being distributed more to the wings as the central peak of the density profile narrows, to achieve $\mathcal{H} = \mathcal{R}$ globally.

2.2.3. The physically complete set of magnetostatic solutions

The set of everywhere-analytical solutions are an extremely restricted subset of the physically-realizable equilibrium states of our thermally-balanced KS slab, a point not previously known. Among the free constant parameters of this set of solutions, γ_0, α_0 and

κ_S define the fixed basic thermal properties of a specific fluid. Another set, B_0 and G_0, fixes the background field. The fluid is a perfect electrical conductor, so its total mass M frozen into the field is a constant in time. Clearly, M can be prescribed arbitrarily for a given set $(\gamma_0, \alpha_0, \kappa_S, B_0, G_0)$ that specifies the nature of the fluid and the intensity of the background field. If the desired equilibrium state is an everywhere-analytical solution, we require $\gamma = \gamma_c = 2/3$ which, by Equations (20), determines $\beta = \beta_c$ where

$$\beta_c = \frac{12\pi\gamma_0 k_B}{\alpha_0 m_0 B_0^2}, \tag{40}$$

completely fixed by the given set $(\gamma_0, \alpha_0, \kappa_S, B_0, G_0)$. By Equation (24), $\beta = \beta_c$ defines a unique equilibrium total mass

$$M_c = \frac{B_0^2}{2\pi}\sqrt{\beta_c}, \tag{41}$$

fixed independent of the above arbitrarily prescribed M. Hence, unless the prescribed M happens to have the value M_c, the prescribed fluid cannot be in an everywhere-analytical equilibrium.

To summarize, if we prescribe $M = M_c$, M_c fix by the given set $(\gamma_0, \alpha_0, \kappa_S, B_0, G_0)$, the fluid in equilibrium has an infinity of everywhere-analytical states available, of different Y dependences, depending on the central temperature $\theta(0) = \theta_1$ as a free parameter. Each of these equilibrium states is the end state of an evolution from some prescribed initial state, governed by the time-dependent extensions of the static equations (13), (14) and (19). The total mass $M = M_c$ is a constant in that evolution. The central temperature θ_1 defines a minimum amount of internal energy retained for each piece of the equilibrium plasma. The $\theta_1 = 0$ equilibrium state is the lowest energy state, a preferred end state in the sense that any higher-energy $\theta_1 \neq 0$ equilibrium state may evolve in response to perturbations by losing energy. If $\theta_1 \neq 0$, the equilibrium D is finite, and $P = D\theta_1 = 1$ at $Y = 0$. As $\theta_1 \to 0$ parametrically, $D(Y)$ as a function of Y becomes unbounded at $Y = 0$, diverging as $D \approx Y^{-\nu}$ with a constant power $0 < \nu < 1$. In that limit, $D(Y)$ not a Dirac delta function in the neighborhood of $Y = 0$. That is to say, the integral of $D(Y)$ over a small interval $-Y_0 < Y < Y_0$ goes to zero as $Y_0 \to 0$.

The interesting new point is that, for *all other* prescribed $M \neq M_c$ with $\beta \neq \beta_c$, a contradiction arises if we demand that the equilibrium state is everywhere analytic. Neither the boundary conditions nor the freedom to arbitrarily prescribe M can be compromised. The physics of the governing ordinary differential equations (ODEs) are also not in question. Physics avoids the implied contradiction by admitting discontinuous solutions, known as weak solutions to ordinary and partial differential equations (Courant & Hilbert 1962). The continuous parts of a weak solution are described by the governing ODEs, whereas the same

physics governs the discontinuities by the integral version of these ODEs. The equilibrium states of a fluid specified by a given set $(\gamma_0, \alpha_0, \kappa_S, B_0, G_0)$ are thus generally singular. Using set-theory language, the infinite set of continuous equilibrium states with $M = M_c$ is a subset of measure zero of all the physically admissible states.

3. Equilibrium with a cold mass sheet

The inviscid, compressible, supersonic flow past a fixed obstacle is a familiar example of inevitable singularities in solutions to partial differential equations. The flow must be sub-sonic in the vicinity of the obstacle to enable the fluid to self-communicate and navigate steadily around the obstacle. A shock front must generally be present where the supersonic flow changes discontinuously to a subsonic flow governed by the integral version of the ideal hydrodynamic equations, the Rankine-Hugoniot equations. This surface of discontinuity can be resolved into a continuous layer of finite thickness if we introduce additional physics significant only in that layer. For example, the introduction of a weak viscosity resolves the shock front into a layer of a thickness determined by the strength of the viscosity. The singular KS-slab solutions presented in this Section are analogous. The everywhere-analytical continuous solutions, requiring a single fixed total mass $M = M_c$, are physically just too restricted. We first survey the singular solutions to understand their physical meaning. In the next Section, we address the additional physics one might consider to account for the internal structure of the singularity.

3.1. The complete absence of equilibrium

Before proceeding, we should point out the case of complete absence of equilibrium for a KS-slab. If radiation is absent, in the limit of $\gamma \to \infty$ in Equation (19), there is no steady state because the unbalanced heat input must everywhere increase the temperature in time. In the opposite extreme, if heating is absent, with $\gamma \to 0$, there is only one singular steady state. The fluid simply radiates away what heat it happens to possess to reach zero temperature, collapsing its entire mass M into a sheet of zero thickness; see the isothermal solutions in Section 2.2.1.

When both radiation and heating are present, the total mass M critically determines whether energy balance is possible. In equilibrium, the hydrostatic pressure $P(Y)$ supporting the fluid weight along $\mathbf{B}$ must be monotonically decreasing outward from the center of the KS slab. With the fixed heating of the form in Equation (18), this stratification tends to

produce a dominance of radiation around $Y = 0$ and a dominance of heating in the far regions. Therefore stratification must be consistent with a temperature $\theta(Y)$ monotonically increasing with distance away from $Y = 0$, such that its inward thermal conduction brings the excess heat of the far regions to be radiated away by the dense slab center.

Too little mass results in poor radiational loss, and no equilibrium is possible as the unbalanced heat-input keeps the temperature everywhere rising monotonically in time. Too much mass results in the opposite effect, the inability of heating to keep up with the radiational loss due to a high-density massive slab center. We have two possibilities in this case. The entire mass may collapse into single massive sheet in a time-dependent evolution, never attaining a steady state and leaving vacuum outside the sheet. The other possibility is that this collapse takes place but does not involve the entire mass. The collapse takes out just a fraction of the total mass so that the rest of the fluid in the outer layer achieves a spatially-extended steady state. These general expectations are met in the quantitative analysis of our KS slab given below.

3.2. The discontinuous KS-slab solutions

Suppose the KS slab contains a central mass sheet with a total mass $m < M$. The monotonically increasing $B_z = B_0 H(Y)$ jumps from a value $-H_2$ to H_2 upon crossing $Y = 0$ from negative to positive Y. This jump defines a discrete sheet current in the x direction producing a Lorentz force that supports the weight of the sheet,

$$mg = \frac{B_0^2}{2\pi} H_2, \tag{42}$$

similar to the isothermal formula (24). The density distribution $D(Y)$ is a Dirac delta function in the vicinity of $Y = 0$ that accounts for m. In contrast the pressure $P(Y)$ must be everywhere finite, given by Equation (13) to ensure pressure balance with the magnetic field, with $P(0) = 1$ at $Y = 0$. The transformation $-\infty < Y < \infty \;\rightarrow\; -\sqrt{\beta} < H < \sqrt{\beta}$ is thus discontinuous, with the single point $Y = 0$ mapped into the range $-H_2 < H < H_2$, and $0 < Y^2$ mapped into $H_2^2 < H^2 < \beta$.

By converting an integration with respect to Y into its equivalent integration with respect to H, we need to allow for the presence of a delta function where one occurs. The formula (37) for the total heat input $\mathcal{H}$ remains valid in the presence of the sheet of mass m. The total radiative loss needs to be re-calculated,

$$\mathcal{R} \;=\; \int_{-\infty}^{\infty} PDdY$$

$$
\begin{aligned}
&= \frac{2}{\beta}\int_{-\sqrt{\beta}}^{\sqrt{\beta}} PdH \\
&= \frac{2}{\beta}\left(2\int_{H_2}^{\sqrt{\beta}} PdH + \int_{-H_2}^{H_2} PdH\right) \\
&= \frac{2}{\beta^2}\left(2\int_{H_2}^{\sqrt{\beta}} (\beta - H^2)dH + \int_{-H_2}^{H_2} \beta dH\right) \\
&= \frac{4}{3\beta^2}\left(2\beta^{3/2} + H_2^3\right). \qquad (43)
\end{aligned}
$$

Global energy balance $\mathcal{R} = \mathcal{H}$ is then expressed by

$$H_2 = (3\gamma - 2)^{1/3}\sqrt{\beta}, \qquad (44)$$

relating γ to H_2, or, m given by Equation (42). Let us fix the set $(\gamma_0, \alpha_0, \kappa_S, B_0, G_0)$ to specify a fluid of interest. Setting the eigenvalue condition $\gamma = \gamma_c$ yields $H_2 = m = 0$ and $M = M_c$, recovering the everywhere-analytic solutions. Conversely, if $M \neq M_c$, use Equation (24) to fix β in terms of the given M, which goes on to determine a $\gamma \neq \gamma_c$ by Equation (20) and a consistent H_2 by Equation (44). The mapping $-\infty < Y < \infty \;\rightarrow\; -\sqrt{\beta} < H < \sqrt{\beta}$ requires H_2 to be positive and bounded above by $\sqrt{\beta}$. Whether our $M \neq M_c$ construction yields a physical solution depends on whether H_2 meets the aforementioned requirement.

To proceed, introduce a second particular value of $\gamma = \gamma_c' \equiv 1.0$. This value of γ by Equation (20) determines a value $\beta = \beta_c'$, that defines a second critical mass M_c' by Equation (24). The nature of the equilibrium, or absence of equilibrium, depending on the total mass M, can now be distinguished into the ranges : $M > M_c$, $M = M_c$, $M_c' < M < M_c$, and, $M < M_c'$.

If $M > M_c$ and $\gamma < 2/3$, Equation (44) gives a negative H_2 in violation of H_2 falling in the range $0 < H < \sqrt{\beta}$, so equilibrium does not exist even when we allow for a central mass sheet. There is too much mass and the heating cannot keep up with the radiational loss. So the entire mass must collapse to a single mass sheet located at $Y = 0$.

If $M = M_c$, we have $\gamma = \gamma_c = 2/3$, $H_2 = 0$, and the equilibrium solution is everywhere analytical.

If $M_c' < M < M_c$, $\gamma_c < \gamma < \gamma_c'$, $0 < H_2 < \sqrt{\beta}$ and the equilibrium solution exists, discontinuous at $Y = 0$ where a m mass-sheet is located.

If $M < M_c'$ and $\gamma > \gamma_c'$, then Equation (44) gives a $H_2 > \sqrt{\beta}$, in violation of H_2 falling in the range $0 < H < \sqrt{\beta}$. No equilibrium solution exists, even if mass sheets are allowed, the case of the total mass M being too small for radiational loss to balance against heating.

So the KS slab can only remain in a time-dependent state with temperature increasing with time everywhere.

3.3. The $M_c' < M < M_c$ Weak Solutions

To construct an explicit singular solution in the range $M_c' < M < M_c$, the boundary condition (23) at $H = \sqrt{\beta}$ ($Y \to \infty$) imposed on the thermal flux $\mathcal{F}$ requires $H_1 = -\frac{1}{3}\beta^{3/2}(2-3\gamma)$ so that Equation (33) gives

$$\mathcal{F}(H) = \frac{1}{3}\left(\sqrt{\beta} - H\right)\left[H\left(H + \sqrt{\beta}\right) - \beta\,(2-3\gamma)\right]. \tag{45}$$

With the integration constant H_1 fixed, the temperature distribution (34) takes the form

$$\begin{aligned}\frac{3}{5}\beta^2\kappa_0\left(\theta^{5/2} - \theta_1^{5/2}\right) &= -2\beta^{3/2}(2-3\gamma)\left(\sqrt{\beta} - H\right) \\ &\quad + \left[(2-3\gamma)\beta - \Gamma_0\right](\beta - H^2) + \frac{1}{2}(\beta - H^2)^2 \\ &\quad - 2\Gamma_0(2-3\gamma)\beta\log\left(\sqrt{\beta} + H\right),\end{aligned} \tag{46}$$

where the integration constant θ_1 allows for prescribing $\theta(H)$ to have any value at $H = H_2$. The thermal flux $\mathcal{F}$ vanishes at $Y \to \infty$ but is dependent on γ and generally not zero at $Y = 0$, the point corresponding to $H = H_2$. Fig. 5a displays the functional forms of $\mathcal{F}(H)$ constructed, for several representative γ values. We call these functional forms unmodified, having analytically extended each of them from the physical range of interest $0 < H < \sqrt{\beta}$ into the negative H-range.

The $\gamma = \gamma_c = 2/3$ thermal flux is unique, with $H_2 = m = 0$ and satisfying boundary conditions (22) and (23) at $H = 0, \sqrt{\beta}$. So $\mathcal{F}(H)$ is physical and defines an infinity of continuous solutions in the full range $-\sqrt{\beta} < H < \sqrt{\beta}$, ie, $-\infty < Y < \infty$. These solutions all have $M = M_c$ differing in the central temperature $\theta(0) = \theta_1$.

For $\gamma_c < \gamma < \gamma_c'$, the solution is singular, obtained by first truncating off the function $\mathcal{F}(H)$ at the limit $H = H_2$ of the range $H_2 < H < \sqrt{\beta}$ that is now to be identified with $0 < Y < \infty$, for H_2 given by Equation (44). In Fig. 5a, the lines $H = H_2$ are drawn from the abscissa to the respective $\mathcal{F}(H)$ curves in the range $\gamma_c < \gamma < \gamma_c'$. The modified $\mathcal{F}(H)$ located in the interval $-\sqrt{\beta} < H < -H_2$, identified with $-\infty < Y < 0$, is defined by the transformation $\mathcal{F}(-H) = -\mathcal{F}(H)$ as illustrated in Fig. 5b. These two continuous solutions in $Y > 0$ and $Y < 0$ are assured to match the cold, discrete sheet of mass m related by Equation (42) to the jump of $2H_2$ in $H(Y)$ across the sheet.

A weak solution for the $\gamma = 0.7$, with $\beta = 1.0$ and $G_0 = 10.0$, is shown in Fig. 6a. This solution is obtained by integrating Equation (33) with respect to H for $\theta(H)$, using Equation (31), over the range $H_2 < H < \sqrt{\beta}$. From it we obtain the symmetric temperature $\theta(Y)$ in $0 < |Y|$ up to a free central temperature that we set to zero, ie, $\theta(0) = \theta_1 = 0$, where the cold sheet of mass m is located. However, this zero temperature is associated with a finite thermal conductive flux entering the sheet from both sides, in evidence in Fig. 5b showing $\mathcal{F} \neq 0$ at $H = H_2$. In other words, $\theta(Y)$ goes to zero on either sides with an infinite gradient such that $\mathcal{F}$ is finite and nonzero at $Y = 0$.

The central sheet should not be thought of being cold with zero temperature but as the limiting case of a layer cooling to zero temperature, and collapsing during an evolution to achieve equilibrium. The collapse proceeds with density D becoming a Dirac delta function to account for the mass m and with P holding steady at unity. The right hand side of energy-balance equation (19) integrated over the thickness of the sheet gives a constant in time, the steady net loss of energy by the collapsing sheet balanced by the steady inward thermal fluxes on both sides of the sheet. During such a collapse, D increases in the sheet to become a Dirac delta function, temperature decreases to keep $P = 1$, producing a steady net loss. This is the nature of the $2/3 < \gamma < 1$ equilibrium states, in each case taking the macroscopic physics of Equation (19) to remain valid for all time in the interior of the mass sheet. In the next Section an example is given for a collapsing sheet that has a distinctly different internal energy process from the exterior continuous parts of the SK-slab.

4. The interior physics of a discrete mass sheet

To complete our study, we present two alternative interior-models for a mass sheet matching an exterior continuous solution of our KS slab. As a sheet collapses with decreasing temperature and unbounded growth in density at a fixed total mass m, we expect the optically-thin assumption to break down. The nature of heating would also be changed. Heating in the prominence is poorly known or understood, which is the reason for adopting the ad hoc form given by Equation (18), used in earlier prominence modeling works.

For illustration purpose we consider the case of a finite-thickness mass sheet whose interior is optically thick to all radiation, subject to no heating, but maintained by thermal conduction to be isothermal, allowing for the uniform temperature to be as low as it happens to be at the interface with the exterior region. In the exterior, described by our KS-slab solutions, the total heat generated is exactly balanced by the total radiative loss. No thermal flux enters mass sheet. When this sheet is at a sufficiently low temperature, the degree of ionization would be so low that the frozen-in condition must break down. Then, resistive

flows of weakly ionized fluid across the "supporting" magnetic field can take place, the second alternative interior-model that takes us a step closer to the observed prominence with its descending threads and rising bubbles.

4.1. Composite KS-slabs

Consider the case $\gamma = 9/16$, with $\beta = 1.0$ and $G_0 = 10.$, in Fig. 5a, as an example of $M_c < M$, i.e., $\gamma < 2/3$. The unmodified thermal flux $\mathcal{F}(H)$ has two zeros in the range $0 < H < \sqrt{\beta}$, one at $H = \sqrt{\beta}$, imposed by the boundary condition at $Y \to \infty$ and the other at a point at $0 < H = H_3 < \sqrt{\beta}$ given by

$$H_3 = \frac{1}{2}\sqrt{\beta}\,(9 - 12\gamma)^{1/2}\,. \tag{47}$$

By definition $H_3 > 0$ so that the second zero of $\mathcal{F}(H)$ in $0 < H$ exists only if $\gamma < 2/3$. This means that the heat generated in the outer layer $H_3 < H < \sqrt{\beta}$ is entirely radiated away in that layer. In other words, there is enough mass in the system to create an outer layer that is by itself in global energy balance. This layer provides no energy to be transferred by thermal conduction to the inner layer, whatever the latter may be. Integrating Equation (45) we obtain $\theta(H)$ up to a free constant $\theta(H_3) = \theta_1$, the temperature at the interfaces $H = \pm H_3$. In a time-dependent cooling of a $M_c < M$ slab, depending on the nature of its initial state, it is possible for such an outer layer to first form and then stabilize, symmetrically placed on the two sides of $Y = 0$, filling up the regions $|H| > H_3$. The rest of the mass m in $|H| < H_3$ may then exist in two forms which we now specify.

If we define the mass m as a collapsed, discrete mass-sheet at zero temperature, we have

$$mg = \frac{B_0^2}{2\pi} H_3, \tag{48}$$

the equivalence of Equation (42). Then, the monotonically increasing $B_z = B_0 H(Y)$ jumps from $-H_3$ to H_3 across $Y = 0$, with the point $Y = 0$ mapped into the interval $-H_3 < H < H_3$ and the intervals $0 < Y^2$ into the iintervals $H_3^2 < H^2$. We must set the boundary condition $\theta(\pm H_3) = \theta_1 = 0$ for the external solution. A static solution of this kind with $\gamma = 9/16$ is displayed in Fig. 6b. The energy equation (19) applies to the exterior solution but not to the interior of the sheet.

The mass m can also exist as a symmetric, isothermal slab of a prescribed temperature θ_1, of a finite width occupying $-Y_3 < Y < Y_3$, matched continuously into a pair of external solutions of our KS-slab occupying symmetrically in $-\infty < Y < -Y_3$ and $Y_3 < Y < \infty$ subject to the boundary conditions that the exterior temperature $\theta = \theta_1$ at $Y = \pm Y_3$. First

prescribe θ_1 and pick up the value of H_3 from Equation (47) or Fig. 5b for $\gamma = 9/16$. The exterior temperature $\theta(H)$ in $H_3^2 < H^2 < \beta$ is then determined. The picked value of H_3 determines m, sufficient for constructing an isothermal solution that locates $H = \pm H_3$ at a pair of points $Y = \pm Y_3$ in physical space. This isothermal solution then self-consistently matches the outer solutions at $Y = \pm Y_3$ with $\theta(\pm H_3) = \theta_1$ and $\mathcal{F}(\pm H_3) = 0$. The construction is then complete, giving continuous distributions $P(Y)$, $D(Y)$, $\theta(Y)$ and $H(Y)$ over $-\infty < Y < \infty$. Fig. 7 displays 2 solutions computed in this way, all sharing the same M and m but for a set of progressively smaller temperatures θ_1 as indicated. Although a dynamical time-dependent theory is outside the scope of our study, our examples mimic the cooling of the central core of a fixed mass m, holding the total mass M also fixed. As the central isothermal core cools quasi-steadily, that core collapses into a slab of diminishing width, approaching a Dirac delta-function in the limit of $\theta_1 \to 0$. Such a collapse proceeds first out of its optically-thin state into an optically-thick state, and then to extremely low temperatures when the assumptions of high ionization and the frozen-in condition must fail.

4.2. Resistive vertical cross-field flows

In an extremely cold and dense fluid, the electrical conductivity cannot be taken as infinite by two effects, the low degree of ionization and the narrowing of collapsing layer to such a small size that the weak but finite electrical resistivity has become important. If resistivity is significant, the Kippenhahan-Schlüter slab can be extended to include a steady vertical resistive flow. Consider the single-fluid resistive hydromagnetic equations (1) and (2), taking the resistivity η uniform in space for simplicity. In the presence of the simple steady vertical velocity

$$\mathbf{v} = [0, 0, v(y)]\,, \tag{49}$$

the rate of change of momentum on the left hand side of Equation (1) vanishes identically and we recover the force-balance equation (3). We also recover the steady energy transport equation (5). The mass conservation is automatically satisfied. Therefore, each of the magnetostatic solutions investigated in this paper is consistent with the above steady, vertical, resistive flow with $\eta \neq 0$.

The induction equation (2) reduces to a simple second-order ODE which can be integrated once to give

$$v(y) = -\frac{\eta}{\Lambda_0}\frac{dH}{dY} + v_0, \tag{50}$$

where v_0 is an integration constant and Λ_0 is the density scaleheight. In all our solutions $\frac{dH}{dY} \to 0$ as $Y \to \infty$. Therefore, we set $v_0 = 0$ for a system static in the far regions. Combined

with magnetostatic equation (14), we have the velocity

$$v(y) = -\frac{\eta\beta}{2\Lambda_0} D. \tag{51}$$

In this resistive flow the energy released from current dissipation is conserved by the release of gravitational potential energy associated with the steady fall of matter. The prominence-drainage event of Liu, Berger & Low (2012) is thus interesting. The drainage liberates gravitational potential energy. If that drainage is across field lines, the liberated energy manifests, not as an increase in kinetic energy, but as dissipative energy that fuels the radiative loss of the prominence plasma.

Suppose η is small but not zero. Then to a first approximation we neglect η and v. The results of Section 3 have the following significance. Suppose $M > M_c$, static equilibrium is achieved in a relaxation by withdrawing a specific portion m of the given total mass M into a collapsed central sheet. This process implies that the density D grows unboundedly at $Y = 0$. At some point, for any given η small but not zero, the velocity v becomes significant at $Y = 0$ leading to a breakdown of the frozen-in condition in spite of the assumed smallness of η.

For example, consider this resistive flow taking the form

$$v(y) = -\frac{\eta\beta}{2h\theta_1} \mathrm{sech}^2 \frac{\sqrt{\beta}}{2\theta_1} Y, \tag{52}$$

with D given by Equation (26) at the uniform temperature $T = \theta_1 T_0$. We have a vertical down flow that is maximum at $Y = 0$ but decreasing with $|Y|$ exponentially. Use the normalization $T_0 = 10^4$K so that $\Lambda_0 \approx 300$ km. The Spitzer electrical conductivity $\sigma = 2 \times 10^7 T^{3/2}$ s^{-1} gives a resistivity $\eta \approx 3 \times 10^6 \theta_1^{-3/2}$. The peak resistive flow at $Y = 0$ is then of the order of $\frac{\eta\beta}{2\Lambda_0\theta_1} \approx 5 \times 10^{-2} \frac{\beta}{\theta_1^{5/2}}$. To produce a flow of the order of 1 kms^{-1}, would require β large and θ_1 small, e.g., $\beta \approx 10^3$, $\theta_1 \approx 10^{-2}$, implying a highly sheared field and low temperature of the order of $T \propto 10^2$K. Such an extreme condition is the reason for a long-standing pessimistic perception that *steady* resistive slippage of ionized plasmas as the result of the Spitzer conductivity is unimportant. The spontaneous formation of a mass-sheet singularity is a novel example of how precisely this kind of extreme circumstances may develop in the corona under which resistive slippage does become important.

This effect is more interesting as a recurrent time-dependent process. If we neglect the weak resistivity altogether, the frozen-in condition demands for an equilibrium state with a singularity. This singularity generates a resistive flow of an unbounded magnitude until the singularity formation is stopped by current dissipation as a heat source for the cold fluid. The heating can increase the degree of ionization, restoring the frozen-in condition,

whereupon a collapse into a mass sheet is once again initiated. This time-dependent process is worthy of further investigation.

4.3. Ambipolar diffusion in the KS slab

To address the degree of ionization, a two-fluid description is needed (Gilbert, Hansteen & Holzer 2002; Gilbert, Kilper & Alexander 2007; Greenfield, Jokipii & Giacalone 2011). Such a description is necessarily 2D, quite outside the scope of our study, but the following is an interesting closing point to make.

In a 1D slab of weakly ionized plasma, the dominant neutrals are kept from slipping freely across the field by collisions with the ions that tend to be tied to the field. The system cannot remain 1D because there will be diffusion of the neutrals in both Y and Z directions. If we concentrate on the vertical force balance in the central region of a KS-like slab, the following order of magnitude consideration adapted from Spitzer (1978, page 294, eqn. (13-55)) is instructive. Take the ions to be rigidly tied to the locally horizontal field as the neutrals fall steadily vertically across the field lines in the presence of a mutual frictional force. For the neutrals as a fluid, its weight is balanced by the upward frictional force acting on it, denoted by $F_{z,i,n}$. The ions as a fluid experiences the opposite frictional force $F_{z,n,i} = -F_{z,i,n}$ as well as the upward Lorentz force that effectively supports the total weight. Use the Spitzer approximation,

$$F_{z,i,n} = -F_{z,n,i} = \rho_i \rho_n \frac{c_0}{m_0} v(y), \tag{53}$$

where $v > 0$ is the speed of the neutral fluid falling relative to a stationary ion fluid with densities ρ_n and ρ_i, respectively. The parameter c_0 is a thermodynamic constant not greatly sensitive to temperature, ranging in value from 10^{-10} to 10^{-9} cm^3 s^{-1} for a hydrogen gas at temperatures in the range $10 - 10^3$K, and, we recall, m_0 is our notation for the mean molecular weight of the fluid which we shall take to be the hydrogen mass. We also have the vertical balance of forces for the two fluid components:

$$\rho_n g = F_{z,i,n}, \tag{54}$$

$$\rho_i g = F_{z,n,i} + B_0^2 \frac{dH}{dy}. \tag{55}$$

Summing these two equations gives the one-fluid Equation (14) following the canceling of equal and opposite frictional forces.

Substituting for the frictional force in Equation (54) given by Equation (53), we obtain, after a canceling of ρ_n as a common multiplicative factor on the two sides of the equation,

the speed of fall is independent of ρ_n:

$$v(y) = -\frac{g}{N_i c_0}, \tag{56}$$

entirely determined by the number density N_i of the ionized fluid. The speed of fall depends on gravity but it is steady and not of the magnitude of a free-fall speed. A slippage velocity of 2 km s^{-1} is obtained if the ion number density drops to below 10^8 cm^{-3}. Again, this speed of fall would not be significant if not for the principal result of the paper. If no such poorly ionized fluid form, the frozen-in condition would obtain. Then, if the mass frozen in the field is greater than M_c', the collapse of the core of the KS slab would bring the temperature at the center to as low as it takes for the number density of the ions to be reduced to the level where the frozen-in condition is invalid. Heating is produced by the friction force and the flow can be thus quenched when the ionization level is increased. What is interesting is that if the frozen-in condition returns, and the total mass still exceeds M_c', cooling and collapse of the optically thick core recur. The condensation is thus recurrent and not static for these theoretical reasons.

5. Discussion

The vertical descent of prominence threads at less than free-fall speeds has been interpreted in several ways. The large-scale twisted field in the prominence cavity may be evolving with flux-tubes or detached fluxes falling bodily together with their frozen-in plasmas as the result of intermittent magnetic reconnections occurring somewhere else along a flux-tube (Lerche & Low 1980b; Low & Petrie 2005; Petrie & Low 2005; Chae 2010; Haerendel & Berger 2011). van Ballegooijen and Cranmer (2010) proposed that the prominence plasma is flowing under the frozen-in condition in a 3D tangled global field that has a strong vertically-oriented component. In contrast, here we propose a spontaneous breakdown of the frozen-in condition to allow a resistive flow across a local horizontally-oriented field. What seems clear is that all these dynamical processes may occur simultaneously.

Our KS-slab model shows that the nonlinear coupling of force-balance with energy-balance under a rigorous imposition of the frozen-in condition must generally produce a cold, zero-thickness sheet of mass if static equilibrium is to be attained. This mass sheet contains a discrete electric current that generates the Lorentz force supporting the weight of the sheet. In a real plasma of a high but finite electrical conductivity, this discrete current must dissipate resistively. In other words, the typically high degree of the frozen-in condition must physically break down within the mass sheet. In a time-dependent relaxation to such an equilibrium, a mass sheet would first develop during the time when the frozen-in condition

applies approximately. Then, in that developing mass sheet, the frozen-in condition soon breaks down to produce a downward resistive flow across the supporting field. Yet, the frozen-in condition is not broken down permanently. The implied resistive heating in the sheet, fueled by gravitational potential energy released by the falling, poorly-ionized plasma, can bring back the frozen-in condition, but only to recreate the circumstance under which a thin, cold sheet is again inevitable. This recurrent spontaneous breakdowns of the frozen-in condition is a physically attractive hypothesis to explain the constantly restless interior of a quiescent prominence as revealed by *SDO*/AIA and *Hinode* observations.

Gravity, anisotropic Lorentz force, optically-thin radiation, heating, and anisotropic thermal conduction all play essential roles in creating what seems quite general circumstances under which thin collapsed mass sheets must form. The particular optically-thin radiative loss and heating described by Equations (17) and (18) are artificial, but they capture basic properties sufficiently well for us to use the KS-slab to demonstrate the inevitability of mass-sheet singularity with mathematical rigor. Our demonstration is surprisingly complete. The mass-sheet singularity in our KS-slab is resolvable into a sheet of finite width using an exact solution for a cross-field resistive flow to account for the breakdown of the frozen-in condition. Both the static and time-dependent problems of this complex coupling are formidable, especially for 2D and 3D systems. Direct numerical simulation holds the only hope for making progress but to be fruitful this approach must start with a physics-based hypothesis like the one presented here. Much further work is needed to treat physically more realistic energy processes for applications directly to the prominence (Gilbert, Hansteen & Holzer 2002; Gilbert, Kilper & Alexander 2007) and other astrophysical systems, notably the interstellar medium (Mac Low et al. 1995; Parrish & Stone 2005).

Collapsed mass sheets may be a common occurrence in the corona. All it takes is a failure to bring energy to where it is needed whenever a particular mode of energy transport becomes over constrained by the coupled requirement of balancing the forces in the gravitationally stratified fluid. Let us conclude with the following intuitive physical picture that has emerged from our study.

In our KS-slab, there are two thermal-insulation mechanisms that can keep the prominence cool against the million-degree hot, thermally highly-conducting corona. The magnetic field is an insulator against thermal conduction across it. Not so well recognized is the self-insulation of the prominence plasma along a flux tube. In a sheared U-shaped flux tube, the frozen-in mass is gravitationally stratified along the tube so as to progressively radiate away the two thermal fluxes conducted inward from the high-temperature upper parts of the tube in the corona. If the total mass is large enough, the steady state may be one in which these thermal fluxes are depleted before the bottom of the tube is reached. Then the bottom

contracts into a cold dense mass simply from want of heat. The degree of ionization of such a core would fall below a threshold whereupon the frozen-in condition must break down.

The prominence/corona transition is similar to the chromosphere/corona transition of the solar atmosphere but that analogy is just imperfect. In the solar atmosphere, the bottom of the chromosphere never cools below about $5000^o K$ because the photosphere beneath it has no bottom and is heated actively by the solar luminosity coming through from below. If the prominence plasma sitting at the bottom of an U-shaped tube has no internal heat source and is self-insulating, it would simply cool to an equivalent of the solar photosphere with a very different property, one with such high density and low temperature as to break the frozen-in condition. This massive core would then flow resistively across the field into the adjacent flux tubes, schematically sketched for a 2D evolving field in Fig. 8. No steady flow is expected, just a recurrent process of the breakdown alternating with restoration of the frozen-in condition by resistive heating.

In realistic 3D situations, the super-cooled core of a prominence plasma slips resistively out of its optically-thin chromospheric cladding into an adjacent flux tube. There it can either continue to slip resistively into other tubes further away or else become so ionized in the new hot environment as to be frozen into the new tube it has just occupied. A sufficiently massive super-cooled core can thus fall through the bottoms of successive U-tubes leaving behind in each of these tubes ionized plasmas at chromospheric temperatures, until the former runs out of mass to remain a collapsed core. A vertical thread of chromospheric plasma is naturally produced; see Fig. 8. The movie of such a process made at the cool chromospheric temperature would then show such a thread forming from out of nowhere with a general downward descent. The presence of U-shaped flux tubes is the pre-requisite of this process.

This process may explain the drainage in a quasi-steady prominence recently reported by Liu, Berger, & Low (2012; see their Fig. 2 and Movie 1(C)). Fig. 9 shows another example, a fresh drainage developing in a slowly moving structure during a prominence eruption on June 13, 2010 investigated by Regnier, Walsch and Alexander (2011). They interpreted the horn-shaped structure in the right subfigure, bright in 171Å and moving out at a moderate speed of about 25 $\mathrm{km\,s^{-1}}$, to be the base of a flux-rope coronal cavity traveling out ahead. This structure has concave-outward, parallel striations presumably due to its U-shaped frozen-in magnetic field. The upper concave-outward boundary of the structure with the dark part of the cavity is sharply defined. An interesting feature not discussed by the authors is the two "dark" wavy parallel threads, revealed as absorption in 171Å in their online movies, that have developed in this moving structure prior to the time 06:32:48 UT of our 171Å snapshot of the threads shown in Fig. 9. Each thread first appears as a blob that immediately elongates and

streams downward to its length seen here. One of the threads at the time of our snapshot is still linked to the central "lowest-point" of the structure's upper sharp boundary where it has originated. Evidently condensation to below $\sim 8 \times 10^5$ K, the peak response temperature of the AIA 171 Å channel of the plasma (Boerner et al. 2012), produces the threads that drain across the U-shaped field at their lowest points. Fig. 8 suggests a resistive possibility for this condensation, providing motivation for a future proper calculation with physical radiative loss and heating applicable to this interesting event.

Although massive, poorly ionized cores are time-dependent objects, our model argues for the presence of prominence plasmas that are more massive, more dense, much colder, and less ionized than currently being contemplated. Perhaps the canonical observation-based numbers describing the prominence, electron density of 10^{10-12} cm^{-3}, temperature of $\approx 5000K$, degree of ionization $0.1 - 10\%$, are *only* the properties of the optically-thin, chromospheric cladding of the not yet observed, transient, optically-thick cores. The tangled-field models of van Ballegooijen and Cranmer (2010) readily give peak densities well in excess of the aforementioned canonical values. These models assume a moderate field of only 10G, whereas even larger densities are implied for fields as high as 60G given by polarimetric observations (Casini et al. 2003; Lopez Ariste & Casini 2003). Our KS-slab suggests that even more extreme densities might occur commonly in prominences.

We emphasize that upward and downward motions accompany this process. The unloading of a flux tube to give mass to the one below results in the former rising by its resultant overcompensating Lorentz force. Correspondingly, the mass-receiving tube below sinks heavily until the Lorentz force of its stretched field can hold it swaying into position. Here is an instance of a flux-tube of fluid rising or falling bodily, carrying its frozen-in magnetic flux along with it. Preliminary observational evidence of such simultaneous motions has recently been detected by *SDO*/AIA (Liu, Berger, Low & Casini 2012, in preparation).

Our hypothesis suggests that the cavity magnetic field supporting the prominence is "porous" in spite of the high electrical conductivity. The observations of Liu, Berger & Low (2011) thus have the significance as a quantitative statement of how porous that magnetic field can be, namely, that an order of magnitude more mass than retained by the prominence at any one time can pass resistively and agitatedly down the magnetic field in a day.

In the second paper we will get a clearer picture of the role of the magnetic field in this process (Low et al. 2012). The field actually is the dominant dynamical player, for it can, on its own, create and restore the frozen-in condition in a permanent restlessness (Parker 1994; Janse & Low 2010; Janse, Low & Parker 2010). This mechanics may be basic to the proposal of Berger et al. (2011) that the long-lived macroscopic prominence is a form of magneto-thermal convection.

We thank Patrick Antolin, Yuhong Fan, Michael Goodman, Phil Judge, Bruce Lites and Gene Parker for discussions. The National Center Atmospheric Research is sponsored by the National Science Foundation. TEB was supported by the Solar-B FPP contract NNM07AA01C at Lockheed Martin. WL is supported by NASA SDO/AIA contract NNG04EA00C.

REFERENCES

Ahn, K., J. Chae, W. Cao, P. R. Goode 2010, ApJ 721, 74

Anzer, U., & P. Heinzel 1999, AA 349, 974

Aulanier, G., C. R. DeVore & S. K. Antiochos 2002, ApJ Lett., 567, L97

Berger, T. E., et al. 2008, ApJ Lett., 676, L89

Berger, T. E., et al. 2010, ApJ 716, 1288

Berger, T. E., et al. 2011, Nature 472, 197

Boerner, P. et al. 2012, Solar Physics, 275, 41

Casini, R., & P. G. Judge 1999, ApJ 522, 524

Casini, R., A. L. Lopez Ariste, S. Tomczyk & B. W. Lites ,2003, ApJ 598, L67

Chae, J., K. Ahn, E.-K. Lim, G. S. Choe, & T. Sakurai 2008, ApJ 689, L73

Chae, J. 2010, ApJ 714, 618

Cottaar, M., & Y. Fan 2009, ApJ 704, 576

Courant, R., & D. Hilbert 1962, *Methods of Mathematical Physics, V. II* (New York: Interscince)

de Toma, G., R. Casini, J. T. Burkepile & B. C. Low 2008, ApJ 687, L123

Dove, J. B., S. E. Gibson, L. A. Rachmeler, S. Tomczyk, & P. Judge 2011, ApJL 731, L1

Fan, Y. 2001, ApJ 554, L111

Fan, Y., & S. E. Gibson 2006, ApJL 641, L149

Fan, Y., & S. E. Gibson 2007, ApJ 668, 1232

Fuller, J., S. E. Gibson, G. de Toma, & Y. Fan 2008, ApJ 678, 515

Gaizauskas, V. 1998, IAU Colloq. 167: New Perspectives on Solar Prominences, 150, 257

Gibson, S. E., & Y. Fan 2006, JGR 111, A12103

Gibson, S. E., T. A. Kucera, et al. 2010, ApJ 724, 1133

Gilbert, H. R., V. H. Hansteen, & T. E. Holzer 2002, ApJ 677, 464

Gilbert, H. R., G. Kilper, & D. Alexander 2007, ApJ 671, 978

Greenfield, E. J., J. R. Jokipii & J. Giacalone 2011, in *The Physics of Partially Ionized Gas with Applications to Processes in the Interstellar Medium*, AIP Conf. Proc. 1366, 115

Heasley, J. N., & D. Mihalas 1976, ApJ 205, 273

Heinzel, P., B. Schmieder et al. 2008, ApJ 686, 1383

Haraendel & T. E. Berger 2011, ApJ 731, 82

Hillier, A., H. Isobe, K. Shibata & T. Berger 2011, ApJ 736, L1

Janse, Å. M., & B. C. Low 2010, ApJ 722, 1844

Janse, Å. M., B. C. Low & E. N. Parker 2010, Phys. Plasmas 17, 092901

Judge, P. G., B. C. Low, & R. Casini 2006, ApJ 651, 1229

Karpen, J. T., & Antiochos, S. K. 2008, ApJ 676, 658

Karpen, J. T., S. K. Antiochos, & Klimchuk 2006, ApJ 637, 531

Kippenhahn, R., & A. Schlüter 1957, Z. Astrophys. 43, 36

Labrosse, N., P. Heinzel, J.-C. Vial, T. Kucera, S. Parenti, S. Gunar, B. Schmieder, & G. Kilper 2010, Space Sci Rev 151, 243.

Lerche, I., & B. C. Low 1980a, ApJ 242, 1144

Lerche, I., & B. C. Low 1980b, Solar Phys., 67, 229-243, 1980.

Leroy, J.-L.1989, in Dynamics and structures of quiescent prominences, ed. E. R. Priest (Dordrecht: Kluwer)

Lin, Y., O. R. Engvold & J. E. Wiik 2003, Solar Phys. 216, 109

Lin, Y., O. R. Engvold, L. R. van der Voort, J. E. Wiik & T. E. Berger 2005, Solar Phys. 226, 239

Lites, B. W., et al. 2010, ApJ 718, 474

Liu, W., T. E. Berger, & B. C. Low 2012, ApJ 745, L21

Lopez Ariste, A. L., G. Aulanier, B. Schmieder & A. Sainz Dalda 2006, AA 456, 725

Lopez Ariste, A. L., & R. Casini 2003, ApJ 582, L51

Low, B. C., 1975, ApJ 198, 211

Low, B. C., 1996, Solar Phys. 167, 217

Low, B. C., 2001, JGR 106, 25141

Low, B. C., & J. R. Hundhausen 1995, ApJ 443, 818

Low, B. C., & G. J. D. Petrie 2005, ApJ 626, 551

Low, B. C., & S. T. Wu 1981, ApJ 248, 335

Low, B. C., & M. Zhang 2004, ApJ 609, 1098

Low, B. C., W. Liu, T. Berger & R. Casini 2011, "The Hydromagnetic Interior of a Solar Quiescent Prominence. II. Hydromagnetic Discontinuities and Cross-Field Mass Transport." , preprint

Luna, M., J. T. Karpen & C. R. Devore 2012, ApJ 746, L30

McIntosh, S. W., H. Tian, M. Sechler, & B. De Pontieu 2012, ApJ, 749, 60

Mackay, D. H., J. T. Karpen, J.L. Ballester, B. Schmieder, & G. Aulanier 2010, Space Sci Rev 151, 333

Mac Low, M., M. L. Norman, A. Königl, & M. Wardle 1995, ApJ 442, 726

Manchester, III, W., et al. 2004, ApJ 610, 588

Marsch, E., H. Tian, J. Sun, W. Curdt & T. Wiegelmann 2008, ApJ, 685, 1262

Martin, S. F., R. Bilimoria & P. W. Tracadas 1994, in *Solar Surface Magnetosm*, eds. R. J. Rutten & C. J. Schrijver (Dordrecht: Academic Publishers)

Martin, S. F., & O. Panasenco 2010, Mm SAI. 8, 662

Okamoto, T. J., S. Tsuneta & T. E. Berger 2010, ApJ 719, 583

Okamoto, J. T., et al. 2007, Science 318, 1577

Okamoto, J. T., et al. 2008, ApJ 673, L215

Parker, E. N. 1994, *Spontaneous Current Sheets in Magnetic Fields* (New York: Oxford U Press)

Parrish, I. J., & J. M. Stone 2005, ApJ 633, 334

Petrie, G. J. D., & B. C. Low 2005, ApJS 159, 288

Priest, E. R., A. W. Hood & U. Anzer 1989, ApJ 344, 101

Reeves, K. K., S. E. Gibson, T. A. Kucera, H. S. Hudson, & Kano 2012, ApJ, 746, 146

Régnier, S., & T. Amari 2004, AA 425, 345

S. Régnier, R. W. Walsh, & C. E. Alexander 2011, AA 533, L1

Schmit, D. E. & S. E. Gibson 2011, ApJ 733, 1

Schmit, D. J., S. E. Gibson, et al. 2009, ApJ 700, L96

Spitzer, L., 1962, Physics of fully ionized gas, (New York: Interscience)

Spitzer, L., 1978, Physical processes in the interstellar medium, (New York: Interscience)

Su, Y., V. Surges et al. 2011, ApJ 734, 53

Tandberg-Hanssen, E. 1995, The nature of solar prominences (Dordrecht: Kluwer)

Tomczyk, S., G. L. Card et al. 2008, Solar Phys. 247, 411

Trujillo Bueno, J., et al. 2002, Nature 415, 403

Uchida, Y. 1963, PASJ 15, 65

van Ballegooijen, A. A. 2004, ApJ 612, 519

van Ballegooijen, A. A., & S. R. Cranmer 2010, ApJ, 711, 164

Wu, F., & B. C. Low 1987, ApJ 312, 431

Xia, C., P. F. Chen, R. Keppens, & A. J. van Marle 2011, ApJ, 737, 27

Xia, C., P. F. Chen, & R. Keppens 2012, ApJ, 748, L62

Zhang, M., & B. C. Low 2005, ARAA 43, 103

Zirker, J. B., Engvold, O., & Martin, S. F. 1998, Nature, 396, 440

Zweibel, E. G., 1982, ApJ 258, L53

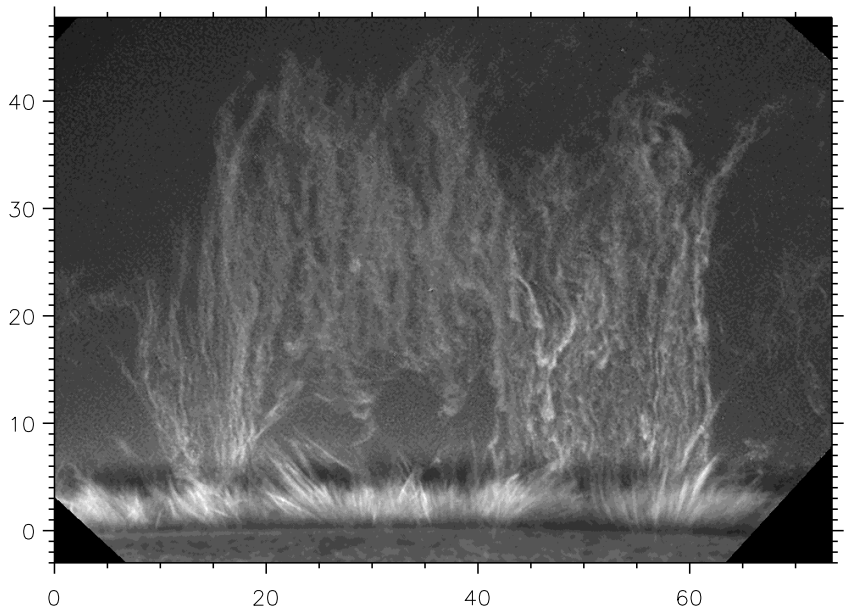

Fig. 1.— A *Hinode*/SOT image in CaII H emission of the fine-scale vertical threads in a prominence observed on October 3, 2007 at the solar limb. The figure is scaled in arc-seconds.

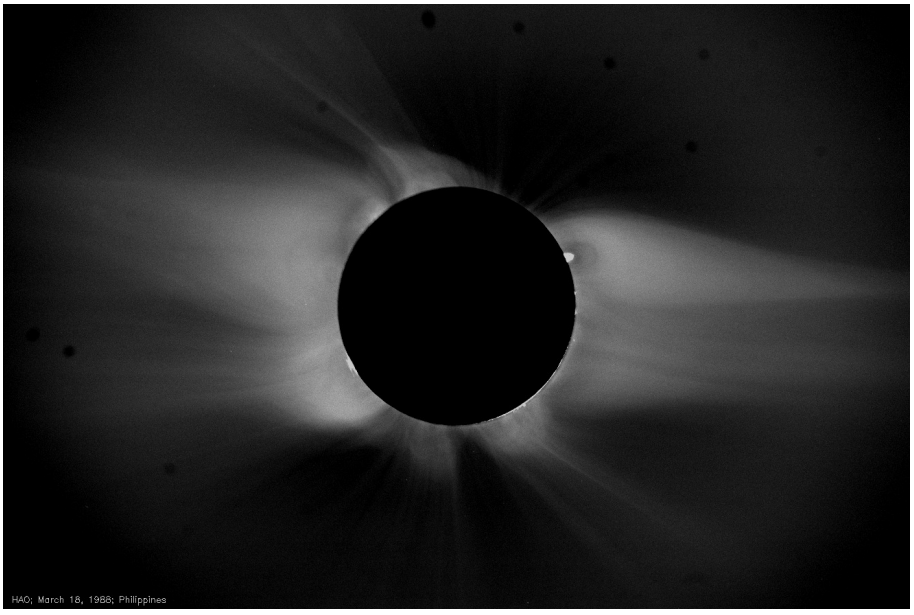

Fig. 2.— White-light total eclipse of March 18, 1988 showing a well-formed, bright coronal helmet-streamer extending from the north-east limb, with a localized, low-density cavity at the helmet base. Within that cavity a spatially-unresolved, quiescent prominence appears as a bright blot.

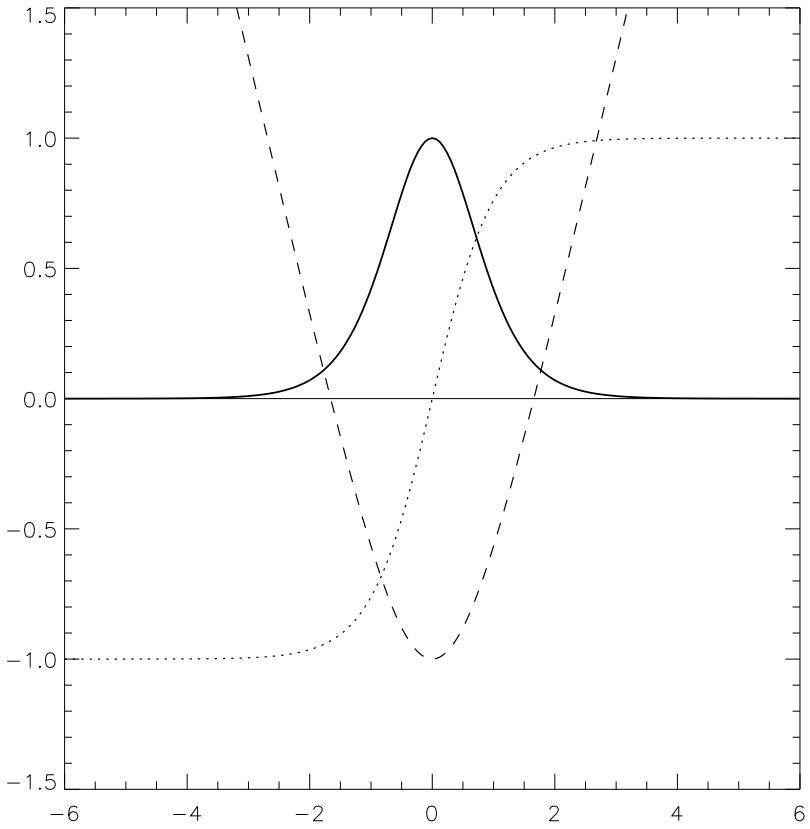

Fig. 3.— An isothermal Kippenhahn-Schlüter prominence slab. Displayed with Y on the abscissa are the density $\theta_1 D(Y)$ (solid), the vertical field-component $\beta^{-1/2} H(Y)$ (dotted), and, the bowed field-line projected on the $Y - Z$ plane (dashed) described by $[Z(Y) + 1]/(2\theta_1)$. The normalization factors fit these curves into a common figure.

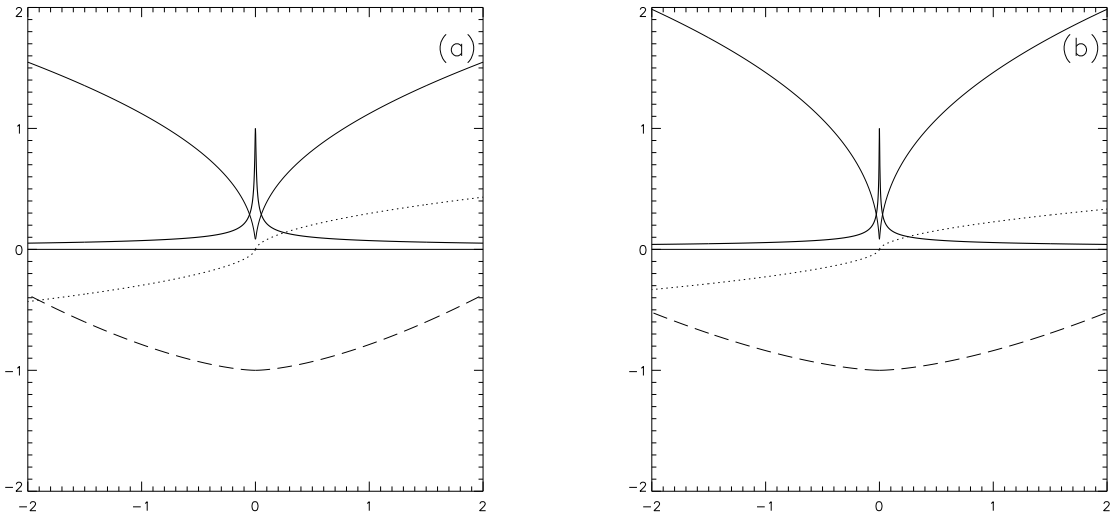

Fig. 4.— Two $\gamma = \gamma_c = 2/3$, thermally-balanced, everywhere-continuous slab solutions, with $\beta = 5.0$, $G_0 = 0$ in case (a) and $\beta = 5.0$, $G_0 = 200.0$ in case (b). Displayed with Y on the abscissa are the density $D(Y)/D(0)$ and the temperature $\theta(Y)/12$, both in solid lines, distinguished by the density having a broad wing and a sharp central peak and the temperature rising monotonically from a locally deep, central minimum. The vertical field-component $2\beta^{-1/2}H(Y)$ (dotted) and the bowed field-line projected on the $Y - Z$ plane (dashed) described by $[Z(Y) + 1]$ show a continuous turn of the field-line at $Y = 0$ resulting from the weight of the central peak density. In case (a) the field lies on the $Y - Z$ plane with $B_x = 0$, whereas in case (b) the highly sheared field with a strong uniform $B_x = B_0 G_0$ has a reduced effective thermal conductivity, leading to a steeper temperature rise from its central minimum and more mass distributed away from the central density peak.

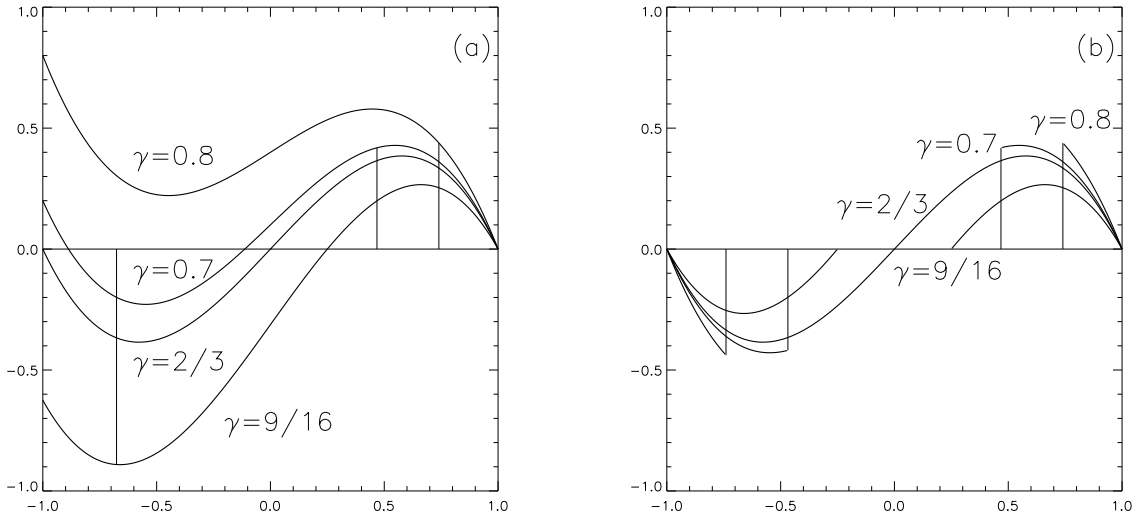

Fig. 5.— The thermal flux $\mathcal{F}(H)$ displayed in the unmodified form (a) and the modified form (b), for four representative cases $\gamma = 9/16, 2/3, 0.7, 0.8 < \gamma_c' = 1.0$, with $-\sqrt{\beta} < H < \sqrt{\beta}$ on the abscissa, described in the text. In (a), the unmodified $\mathcal{F}(H)$ is antisymmetric about $H = 0$ if $\gamma = \gamma_c = 2/3$, giving the only everywhere continuous solution. The other discontinuous solutions are compatible with a collapsed mass-sheet located at $Y = 0$ where the monotonically increasing $H(Y)$ jumps from $-H_2$ to H_2, provided H_2 given by Equation (44) is positive for a self-consistent construction. The vertical lines in (a) identify$H = H_2$ for the three $\gamma \neq \gamma_c$ cases, showing that this construction is possible only for $\gamma = 0.7, 0.8$, for each of which, an antisymmetric modified $\mathcal{F}(H)$ shown in (b) is constructed by truncating the unmodified $\mathcal{F}(H)$ at $H = H_2 > 0$ to define the continuous part of the solution in $H_2 < H < \sqrt{\beta}$ and defining $\mathcal{F}(H) = -\mathcal{F}(-H)$ in $-\sqrt{\beta} < H < -H_2$. The case $\gamma = 9/16$ with $H_2 < 0$ in (a), representative of the regime $\gamma < \gamma_c$, is characterized by having two positive zeros of $\mathcal{F}(H)$, at $H = \sqrt{\beta}$ and $H = H_3 > 0$ given by Equation (47). Its antisymmetric modified $\mathcal{F}(H)$ shown in (b), describes a different model that locates the mass-sheet at $Y = 0$ where $H(Y)$ jumps from $-H_3$ to H_3, described in the text.

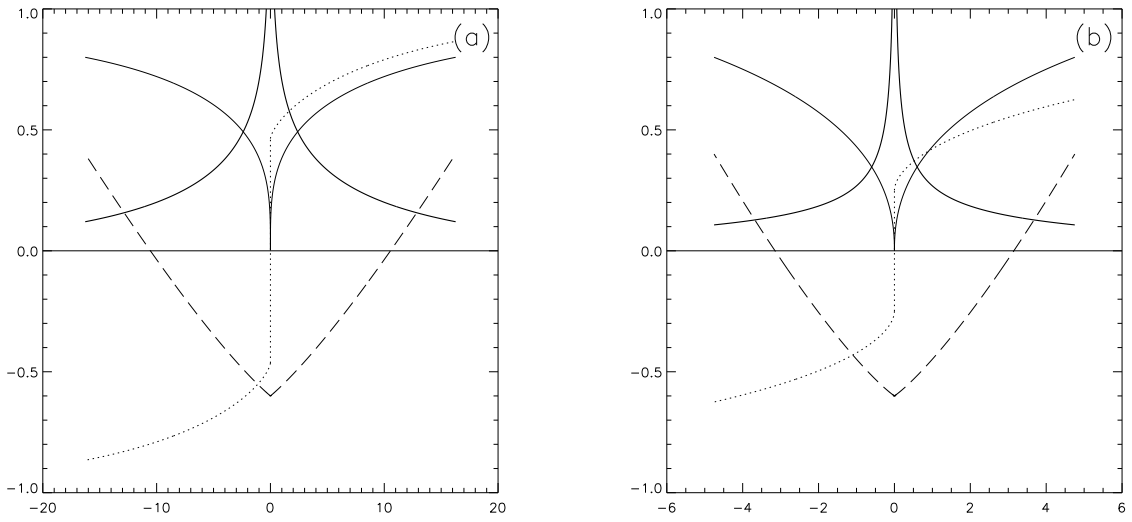

Fig. 6.— Two representative, discontinuous, thermally-balanced slab solutions: (a) $\gamma = 0.7$ and (b) $\gamma = 9/16$, with $\beta = 1.0$, $G_0 = 10.0$ in both cases. In each case, displayed with Y on the abscissa are the density $D(Y)$ with a central δ-function peak and the temperature $\theta(Y)$ monotonically increasing from 0 at $Y = 0$, both graphs in solid lines and suitably normalized to fit into the same figure. The vertical field component B_z is displayed as $H(Y)/\sqrt{\beta}$, the dotted lines, discontinuous at $Y = 0$ with jumps of $2H_2/\sqrt{\beta}$ and $2H_3/\sqrt{\beta}$ for cases (a) and (b), respectively. These jumps give the respective projected field-lines, the dashed lines suitably normalized and positioned to fit into the figures, each a central kink associated with a δ-function current density directed in the x direction. The discrete Lorentz forces of these discrete currents support the weights of the respective mass-sheets, relating their masses to the central jumps in H by Equations (42) and (48), respectively. A nonzero thermal flux passes into the central mass-sheet from both sides in (a), whereas the thermal flux vanishes on both sides of the mass-sheet in (b), as described in the text.

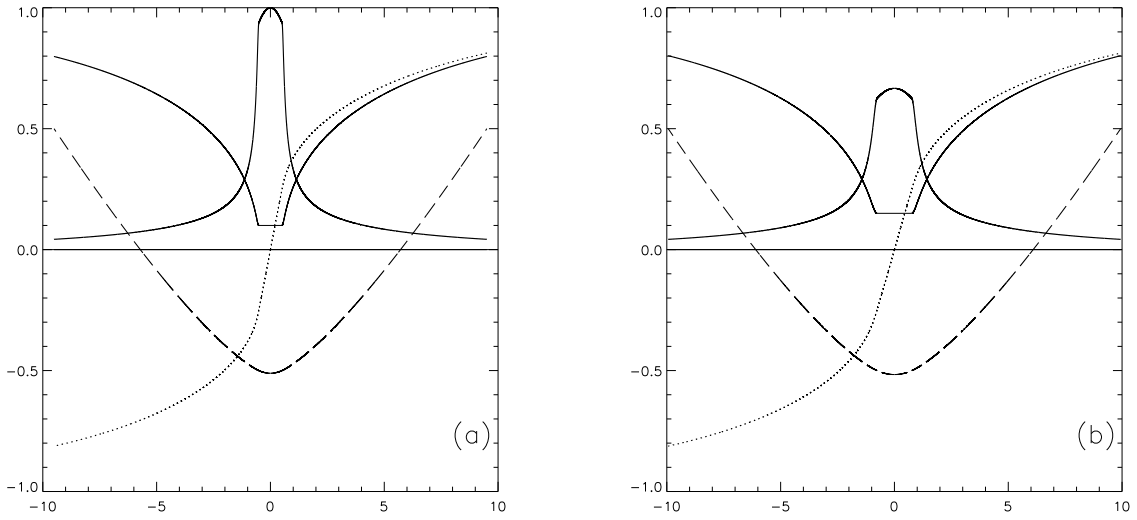

Fig. 7.— Two composite thermally-balanced slab solutions made up of a central isothermal slab continuing at $H = \pm H_3$ into the $\gamma = 9/16$ continuous exterior solutions on the two sides, with $\beta = 5.0$ and $G_0 = 10.0$ for both solutions, the former fixing the total mass M. The line styles used in Fig. 6 to distinguish the different physical quantities are adopted here. The parameters for the two solutions are identical except for the temperature of the central isothermal slab, which is 1.5 times cooler in (a) than in (b). The same normalizations used to fit the graphs in a common figure in each case are not essential. These solutions make the point that the mass-sheet solution in Fig. 6b has an everywhere continuous version in which the mass-sheet is spatially resolved into an isothermal slab of a finite width that is directly proportional to the isothermal temperature. The fluid surfaces $H = \pm H_3$ bound a fixed total mass between them. The lower the isothermal temperature, the spatially closer these two fluid surfaces are, giving rise to a density distribution of mass that tends to a δ-function as the isothermal temperature goes to zero.

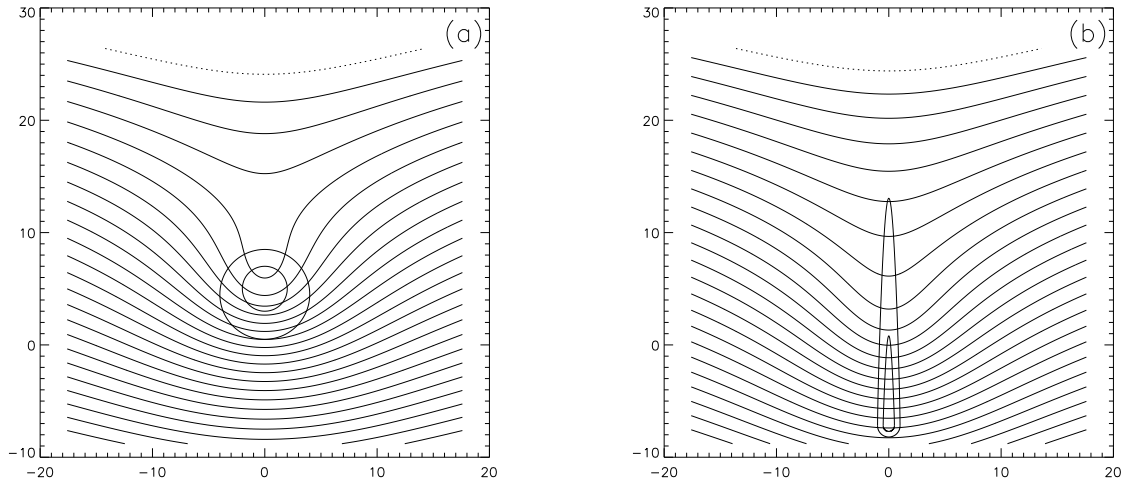

Fig. 8.— Sketch of plasma-condensation dynamics leading to a resistive flow of the collapsed core across a set of locally-bowed 2D magnetic field-lines. In the non-equilibrium initial state (a), a plasma blob is represented by two circular boundaries, the inner boundary containing a cold dense fluid that can move under gravity across the field to lower heights by intermittent resistive effects. Between the two boundaries is a hot fluid sufficiently ionized to be frozen-into the field. As the core fluid moves into the bow field-lines below, its outer shell may be conductively heated and ionized to become frozen into the new flux threaded by the descended fluid. If a sufficient amount of the core fluid remains resistive, it will continue to resistively descend at below gravitational free-fall speeds. The same frozen-in 24 field lines in the end-state (b) is sketched in relation to the initial state (a) to show the respective rising and sinking of lightened and loaded flux-tubes described in the text, resulting in the vertical elongation of the descending condensation as well as a local upward and downward expansion of the local field.

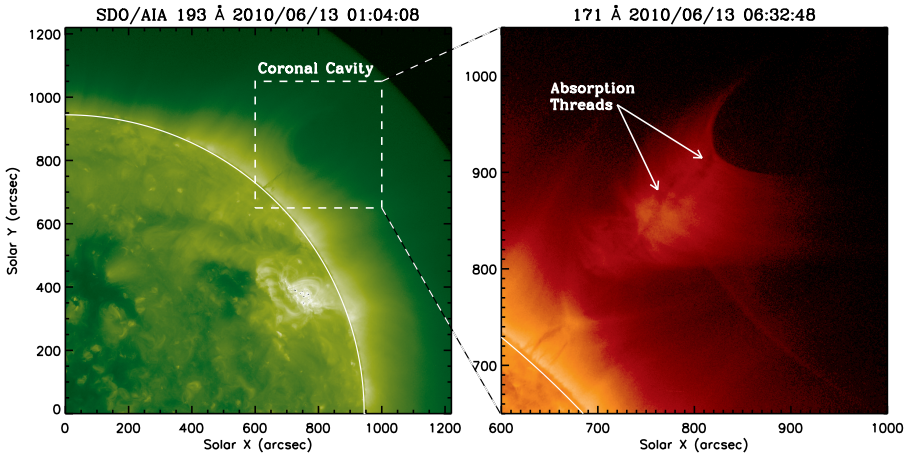

Fig. 9.— The *SDO*/AIA observation of the cool density enhancement at the base of a coronal cavity traveling out at 25 $\mathrm{km\,s^{-1}}$ during the prominence eruption of June 13, 2010 studied by Regnier, Walsh & Alexander (2011). The 193Å image on the left shows the pre-eruption, oval-shaped dark cavity with vertical absorption threads suspended at its base. The 171Å image on the right shows an enlarged view of the boxed region on the left about 5 hours later, revealing two parallel dark absorption threads, newly developing during the eruption and crossing the "lowest-points" of the horn-shaped, concave-outward magnetic striations in emission, suggestive of cross-field drainage of condensed plasma.